Physical and Optical Properties of Aged Biomass Burning Aerosol from Wildfires in Siberia and the Western US at the Mt. Bachelor Observatory

James R. Laing[1], Daniel A. Jaffe[1,2], Jonathan R. Hee[1]

Response to reviewer #1:
We thank the reviewer for their comments on the article. We've responded to the individual comments below.

Summary
The paper summarizes the physical and optical properties of aerosols from biomass smoke from regional to continental scale events. The paper is appropriate, well focused and should eventually be publishable in ACP. I recommend the following minor modifications and additional analysis prior to publication.

Technical Comments

Techniques and analysis seem sound. The criteria for smoke impacts and differentiating LRT and regional smoke events with water vapor seems well-thought out.

Certainly the trend is consistent of lower SSA for the Siberian fires and thus a flaming, higher MCE fire. However, all the SSA values are all relatively high suggesting an MCE on the lower end of the range (mixed to smoldering combustion). This is worth commenting. For reference see the Liu paper below.
Response: This is a good point as all of the SSA's we observed were >0.95, but low SSA values seem to be only observed in studies of primary emissions. Vakkari et al. (2014) and Yokelson et al. (2009) observed SSA to increase significantly with aging in wildland fire plumes within an hour of emission. In addition, at MBO Briggs et al. (2016) found that BB plumes do not follow the SSA vs MCE parameterization from Liu et al. (2014) and that all SSA values were >0.92 despite very high MCE values. These high SSA values were attributed to SOA formation and increased scattering efficiency driven by particle growth. Given this and that fact that MCE couldn't be accurately derived due to the high CO2 background, I'm hesitant to say that the equate the relatively high SSA values for the Siberian plumes, which have been atmospherically processed for up to 10 days, to mixed to smoldering combustion.
I have added a paragraph to address this in Section 3.3 (Lines 302-315).

The analysis brought to mind a recent paper by the CSU group examining emitted and aged biomass smoke sizing and radiative properties paper referenced below which may provide a useful intercomparison and context.
Response: The Carrico et al. (2016) paper is a useful paper to compare with our paper. We cited it in comparison with our results for size distributions in Line 388.

Table 1 is useful, however would be more useful with the following additions:
- A summary mean +/- s.d. for the regional versus Siberian events, maybe 2 lines at the bottom
Response: This is a good idea and was added to Table 1.

- Adding in your rough estimate of the age of the plume for each case which was stated as a range elsewhere. ***Do the size distributions with Aitken modes correspond to the younger plumes? Are there any other conclusions to be drawn?***
Response: We looked into this but it was too ambiguous to draw any definitive conclusions. Most of the regional BB events were influenced by multiple fires which made it nearly impossible to properly estimate plume age. Additional language to explain this was added in Section 3.2 (Lines 256-260), and Figure 3 was added for a visual explanation.
As far as the events with bimodal distributions, 3 of the 5 are of Siberian origins. Given this we suspect the Aitken mode in these size distributions most likely represents a secondary source from within the boundary layer. We have put this in Line 371.

Figure 4. I'm not sure how the percentiles are done with such small numbers of samples, symbol with whiskers showing the range seems more appropriate. You're really comparing the Siberian to regional fires, why separate into 3 groups? I could only see one small outlier symbol on the chart.
Response: Figure 4 (now Figure 5) was changed to 2 groups, Siberian and Regional fires. Due to the outlier for the Siberian BB AAEs we feel the box plots give a more accurate portrayal of the distribution on the values rather than a mean and whiskers showing the range

Figure 5. Meaning of this? The events symbols are not distinguishable; I would simply delineate Siberian vs. regional with different symbols and colors. With the exception of CO, these parameters are by definition or calculation interdependent. Is the take home message something along the lines of, "Biomass smoke events as indicated by elevated CO concentrations featured shifts to larger sizes driving higher PM mass concentration, light scattering coefficients, and the highest overall mass scattering efficiencies."
Response: Figure 5 was removed and replaced with Figure 7, which is a similar plot but with D_{pm} on the x-axis. This looks at the dependence of different variables on size distribution instead of MSE. For Figure 7 all the events were changed to the same color and not individually identified since D_{pm} was shown not to depend on transport time.
The previous plots showed a correlation between MSE and σ_{scat}, PM1, and CO, all of which can be thought of as surrogates for plume concentration. Since σ_{scat}, PM1, and CO are all correlated with size distribution (Figure 7), the correlations with MSE are likely just a function of particle size and cause no causal effect. In summary it seems the more concentrated the BB plume (higher σ_{scat}, PM1, CO) the larger the size distribution, which in turn increases the MSE.
Given this, we decided to highlight the correlation between σ_{scat}, PM, CO versus Dpm instead of MSE.
Language regarding the new figure is in Lines 350-357, and 390-398.

Mechanics and Presentation

The presentation is appropriate in terms of length, style and diction. Figures are appropriate.

Why put the hysplit trajectories plot in supplementary material though? The CALISPO images are appropriately in the supplement. However, the paper is short enough it can accommodate the additional figure rather than the annoyance of looking elsewhere.
Response: This Figure was moved to the main manuscript. It is now Figure 6.

I noted a few inconsistencies (line 158 and 196 for example) in variable, citation, and subscript italics, check throughout.
Response: The manuscript was checked for inconsistencies and proofread.

Line 109 "was located prior to any. . .." Aerosol instrumentation?
Response: This was changed

Line 133, I recommend breaking out as an equation rather than inline.
Response: This was changed

Line 192, I believe you mean Period 2.
Response: This was changed

Line 209, "ascended from the boundary layer (BL) to. . .." MBO?
Response: This was changed

Line 242 superscript missing
Response: This was changed

Line 280 "hygroscopy" replace with hygroscopicity Line 299 "Mei" replace with Mie
Response: This was changed

Line 375 "preformed" replace with performed
Response: This was changed

Response to reviewer #2:
We thank the reviewer for their comments on the article. We've responded to the individual comments below.

This manuscript characterizes the physical and optical properties of biomass burning aerosols transported over the Mt. Bachelor Observatory during the summer 2015. This is an important dataset and deserves to be published. This being said, I feel the analysis of the measurement data could have been better processed with appropriate uncertainty values assigned. Hence, I would recommend publication of this manuscript after mandatory revision. Below are my major comments:

1) The fact that the authors observe a low single scattering albedo and Absorption Angstrom exponent implies majority of the aerosols were black carbon (BC) and not Brown Carbon. This is corroborated by higher MCE values indicating flaming phase of combustion. So, my question is: why are the authors surprised at lack of BrC aerosols? BrC aerosols are generated from smoldering fire phase, mostly associated with peat burning. Smoldering phase is associated with very low MCE, which was not observed in this study. What the authors observed were over crown forest fires (flaming phase). This concept has to be made clear in the text and the abstract. Otherwise, the confusion that only BC is generated from Siberian forest fires would propagate in the community.
Response:
We explain why we suspect there is a lack of BrC in the Siberian events in Section 3.3 (Lines 316-330). We explain that the lower AAE values could be due to a lack of BrC initially produced by the fires due to flaming conditions. We also suggest that the low AAEs could be due to the loss of BrC during transport through photobleaching, volatilization, and aerosol-phase reactions. We were not able to calculate MCE due to the long transport times, low CO2 enhancements and high background. We do state in the abstract (Line 23), results (Lines 279-283), and conclusions (Lines 422-427) that we suspect the Siberian events represent a selective portion of the fire plume that is more likely to represent flaming conditions.

2) The abstract and the text says "aerosol light scattering and absorption" were measured. Please specify what parameters were measured, scattering and absorption cross-sections or coefficients? I am assuming the authors measure coefficients.
Response: We measured scattering and absorption coefficients. We have clarified this in Line 21, 89, 106, 118, and 203.

3) The scattering and absorption coefficients were adjusted to desired wavelengths using Ansgtrom exponents calculated by other studies. Could the authors specify the values used to extrapolate? Reading Fisher et al (2010), it seems the SAE values ranged between 2-2.8? What's the rationale behind using this range? Why not use 4 instead? Since all particles are in Rayleigh regime (sub-micron), their scattering cross-sections decrease in power-law exponents of 4 with increasing wavelength. So, why did the authors adopt SAE of 2.4 and not 4?
Response: The SAE values were calculated for each 5-min average using the scattering coefficient measurements at 450 nm and 550 nm. We then used this SAE for each 5-min period to adjust the scattering coefficient measurement at 550 nm to 528 as per equation 1. This was

done so we could calculate single scattering albedo from scattering and absorption measurements at the same wavelength. This has been clarified in the manuscript in Lines 142-152.

4) Figure 5 doesn't make any sense to me. Could the authors provide any physical explanation behind the correlations? Scattering in the Rayleigh regime goes as square of particle volume, which probably explains the poor correlation. But what about the others. If one cannot explain or even hypothesize the reason behind a plot, why put it. I suggest the authors to remove this unnecessary plot from the main manuscript or move it to Supplementary Materials.

Response: Figure 5 was removed and replaced with Figure 7, which is a similar plot but with D_{pm} on the x-axis. This looks at the dependence of different variables on size distribution instead of MSE. For Figure 7 all the events were changed to the same color and not individually identified since D_{pm} was shown not to depend on transport time.

The previous plots showed a correlation between MSE and σ_{scat}, PM1, and CO, all of which can be thought of as surrogates for plume concentration. Since σ_{scat}, PM1, and CO are all correlated with size distribution (Figure 7), the correlations with MSE are likely just a function of particle size and cause no causal effect. In summary it seems the more concentrated the BB plume (higher σ_{scat}, PM1, CO) the larger the size distribution, which in turn increases the MSE. Given this, we decided to highlight the correlation between σ_{scat}, PM, CO versus Dpm instead of MSE.

Language regarding the new figure is in Lines 350-357, and 390-398.

5) Please provide an error analysis of the techniques used to measure absorption and scattering coefficients. Uncertainties involved during calculation of SAE, AAE using previously published data should be mentioned. A paragraph on error analysis is a must for this kind of study. I would further suggest to propagate these values to the error bars in figure 4.

Response: An error analysis was completed. Precision and total uncertainties were calculated for all of the optical measurements and provided in Table S1. We added description of the error analysis in the Methods Section. Lines 212-128 for aerosol scattering, Lines 135-142 for aerosol absorption, Line 156 for AAE, Lines 185-198 for enhancement ratios.

6) The manuscript has grammatical and typographical errors. I suggest a thorough editing done to the contents during its revision.

Response: We went through the paper and corrected any grammatical and typographical errors. We also checked for consistency.

Physical and Optical Properties of Aged Biomass Burning Aerosol from Wildfires in Siberia and the Western US at the Mt. Bachelor Observatory

James R. Laing[1], Daniel A. Jaffe[1,2], Jonathan R. Hee[1]

[1] University of Washington Bothell, Bothell, WA, USA
[2] University of Washington, Seattle, WA, USA

Correspondence to: Daniel A. Jaffe (djaffe@uw.edu)

Abstract. The summer of 2015 was an extreme forest fire year in the Pacific Northwest. Our sample site at the Mt. Bachelor Observatory (MBO, 2.7 km a.s.l.) in central Oregon observed biomass burning (BB) events more than 50% of the time during August. In this paper we characterize the aerosol physical and optical properties of 19 aged BB events during August 2015. Six of the nineteen events were influenced by Siberian fires originating near Lake Baikal that were transported to MBO over 4-10 days. The remainder of the events resulted from wildfires in Northern California and Southwestern Oregon with transport times to MBO ranging from ~~4.5~~3-35 hours. Fine particulate matter (PM1), carbon monoxide (CO), aerosol light scattering coefficients (σ_{scat}), aerosol light absorption coefficients (σ_{abs}), and aerosol number size distributions were measured throughout the campaign. We found that the Siberian events had a significantly higher $\Delta\sigma_{abs}/\Delta$CO enhancement ratio, higher mass absorption efficiency (MAE; $\Delta\sigma_{abs}/\Delta$PM1), lower single scattering albedo (ω), and lower Absorption Ångström exponent (AAE) when compared with the regional events. We ~~suspect~~ suggest that ~~the~~ the observed Siberian events ~~observed~~ represent that~~a~~ portion of the ~~fire~~ plume that has hotter flaming fire conditions and thus~~that~~ enabled strong pyro-convective lofting and long-range transport to MBO. The Siberian events observed at MBO therefore~~do not~~ represent a selected portion of the original plume that would then have preferentially higher black carbon emissions and thus an enhancement in absorption~~ enhancement~~. The lower AAE values in the Siberian events compared to regional events indicate a lack of brown carbon (BrC) production by the Siberian fires or a loss of BrC during transport. We found that mass scattering efficiencies (MSE) for the BB events ranged from 2.50-4.76 m^2 g^{-1}. We measured aerosol size distributions with a scanning mobility particle sizer (SMPS). Number size distributions ranged from unimodal to bimodal and had geometric mean diameters (D_{pm}) ranging from 138-229 nm and geometric standard

Formatted: Font: Not Italic

Formatted: Subscript

deviations (σ_g) ranging from 1.53-1.89. We found MSEs for BB events to be positively correlated with the geometric mean of the aerosol size distributions (R^2 = 0.73), which agrees with Mie Theory. We did not find any dependence on event size distribution to transport time or fire source location.

Formatted: Subscript

1. Introduction

Biomass burning (BB) is a major source of aerosol in the atmosphere [*Andreae and Merlet*, 2001; *Bond et al.*, 2004]. BB particles are predominantly organic carbon (OC) and black carbon (BC), with some inorganic material [*Reid et al.*, 2005b; *Vakkari et al.*, 2014]. These particles can significantly impact the Earth's radiative balance and climate through direct and indirect aerosol effects. The direct effects on radiative forcing are due to the light scattering and absorption of the aerosol [*Boucher et al.*, 2013; *Haywood and Boucher*, 2000], and the indirect effects are caused by particles acting as cloud condensation nuclei (CCN) which affects cloud albedo [*Pierce et al.*, 2007; *Spracklen et al.*, 2011]. According to the IPCC 2013 report the largest uncertainty in determining global radiative forcing comes from quantifying the direct and indirect effects of aerosols [*Boucher et al.*, 2013]. Biomass burning is a major contributor to global aerosol burden and it has been predicted that these emissions are likely to increase due to climate change, particularly in the boreal forests of North America and Russia [*Flannigan et al.*, 2009; *Stocks et al.*, 1998] and in the w~~W~~estern US [*Y Liu et al.*, 2014b; *Westerling et al.*, 2006]. This makes the proper characterization of aged BB emissions even more important.

Currently there are few field measurements of well-aged BB emissions. Our knowledge of BB aerosol primarily comes from laboratory experiments and near-field measurements taken within a few hours of a wildfire [*May et al.*, 2015; *May et al.*, 2014; *Okoshi et al.*, 2014; *Vakkari et al.*, 2014; *Yokelson et al.*, 2013b; *Yokelson et al.*, 2009]. *Holder et al.* [2016] showed that laboratory measurements of aerosol optical properties do not accurately reproduce field measurements. Freshly emitted BB particles are small in diameter (30-100 nm) [*Hosseini et al.*, 2010; *Levin et al.*, 2010]. As the plume ages, the aerosol undergoes rapid chemical and physical changes on the time scale of minutes to hours [*Reid et al.*, 2005a; *Reid et al.*, 2005b; *Vakkari et al.*, 2014]. The change in particle size is due to coagulation and the condensation of organic material onto the existing particles [*Reid et al.*, 2005b; *Seinfeld and Pandis*, 2006]. The

coagulation rate can be very high in fresh BB plumes since this is equivalent to the square of particle number concentration. This process increases the size of the particles while decreasing the number concentration. Condensation of secondary organic aerosol (SOA) onto particles in BB plumes ~~can~~ also increases particle size. The condensation of SOA is counterbalanced by the loss of primary organic aerosol (POA), which can evaporate during plume dilution [*May et al.*, 2015; *May et al.*, 2013]. The net condensation/evaporation effect is highly variable. Some studies have observed an increase in mass with plume age due to SOA production [*Briggs et al.*, 2016; *Hobbs*, 2003; *Vakkari et al.*, 2014; *Yokelson et al.*, 2009], while others have observed limited SOA formation [*Akagi et al.*, 2012; *Jolleys et al.*, 2015]. All of these uncertainties in the aging process of biomass burning underscores the importance of characterizing the physical and optical properties of well-aged biomass burning aerosol.

In this study we analyze ~~the physical and optical aerosol properties of~~ 19 aged BB events observed in the summer of 2015 at Mt. Bachelor in Oregon. The BB events consisted of ~~R~~Regional events (fires in Northern California and Southwestern Oregon; transported 3-3~~5~~0 hours) and Siberian fire events (fires around Lake Baikal; transported 4-10 days). We investigated the aerosol optical and physical properties of these events and explored their variation with source location and transport time. This study addresses the following questions:

- What are the differences in the optical properties of regional and Siberian BB events observed at MBO?
- What is the range of mass scattering efficiencies for BB events and what explains their variability?
- What is the range in aerosol size distributions of BB events at MBO and how does this vary with plume age?

2. Methods

2.1. Mt. Bachelor Observatory

The Mt. Bachelor Observatory (MBO) is a mountaintop site that has been in operation since 2004 [*Jaffe et al.*, 2005] . It is located at the summit of Mt. Bachelor in central Oregon, US (43.98° N, 121.69° W, 2,764 m a.s.l.). A suite of measurements (including carbon monoxide (CO), ozone (O_3), aerosol scattering coefficients, and more) have been made continuously at the

summit site ~~since 2004~~. Previous studies have observed BB plumes in the free troposphere from regional and distant sources in the spring, summer, and fall [*Baylon et al.*, 2015; *Briggs et al.*, 2016; *Collier et al.*, 2016; *Timonen et al.*, 2014; *Weiss-Penzias et al.*, 2007; *Wigder et al.*, 2013], and long-range transport of Asian pollution in the spring [*Ambrose et al.*, 2011; *Fischer et al.*, 2010a; *Fischer et al.*, 2010b; *Gratz et al.*, 2014; *Jaffe et al.*, 2005; *Reidmiller et al.*, 2010; *Timonen et al.*, 2014; *Timonen et al.*, 2013; *Weiss-Penzias et al.*, 2006]. During the summer of 2015 an intensive field campaign was performed at MBO to measure aerosol physical and optical properties of wildfire emissions.

2.2. CO, CO_2, and Meteorological Data

CO and CO_2 measurements were made using a Picarro G2302 Cavity Ring-Down Spectrometer. Calibrations were performed every 8 hours using three different NOAA calibration gas standards, which are referenced to the World Meteorological Organization's (WMO) mole fraction calibration scale [*Gratz et al.*, 2014]. Total uncertainty based on the precision of calibrations over the campaign was 3%. Basic meteorology measurements, such as temperature, humidity and wind speed were also measured continuously [*Ambrose et al.*, 2011].

2.3. Aerosol Instruments

We measured dry (relative humidity (RH) less than 35%) aerosol scattering and absorption coefficients, aerosol number size distribution, and particle mass during the 2015 summer campaign in 5 minute averages. An inline 1 µm impactor was located prior to the aerosol instruments. The aerosol instruments were located in a temperature-controlled room within the summit building, situated approximately 15 m below the inlet. ~~A 1 µm impactor was located inline prior to any~~The ~~The~~ aerosol sample line was situated such that the last 2.5 m was located within a space that was temperature controlled at 20 ± 3°C, typically 10°C–20°C warmer than ambient. Relative humidity of the sampled air was less than 35% throughout the campaign. The temperature increase from going outside into the heated building reduced the RH of the sample. RH was measured in the sample airstream by the nephelometer and SMPS. The average RH during the campaign measured by the nephelometer and SMPS was 22.1% and 22.6%, respectively. Ninety--five percent of the 5 minute averaged samples had an RH less than 30%.

We measured multi-wavelength aerosol light scattering coefficients (σ_{scat}) using an integrating nephelometer (model 3563, TSI Inc., Shoreview, MN) at wavelengths 450, 550, and 700 nm. During the 2015 campaign the TSI nephelometer was periodically switched to measure both particle free air and CO_2. The measured values were corrected for offset and calibration drift in addition to angular ~~nonidealities~~ nonidealities [*Anderson and Ogren*, 1998]~~[Anderson and Ogren, 1998].~~. The filtered air and CO_2 were measured approximately every two ~~weeks~~weeks [*Anderson and Ogren*, 1998]. ~~[Anderson and Ogren, 1998].~~ The data reduction and uncertainty analysis that we followed for the scattering data are outlined ~~by~~ by *Anderson and Ogren* [1998]. ~~Anderson and Ogren [1998].~~ Sources of uncertainties associated with the nephelometer include photon counting noise, zeroing and calibration, and the correction for angular nonidealities. Combined these uncertainties ~~errors~~ yielded ~~a~~ total uncertainties~~y~~ of ~15~~±8~~% during BB events.~~for a scattering coefficient of 30 Mm−1, a 60 min averaging time and a wavelength of 550 nm~~

We measured aerosol light absorption coefficients (σ_{abs}) with a 3λ tricolor absorption photometer (TAP, Brechtel Inc., Hayward, CA) at wavelengths 467, 528, and 660 nm. Throughout the paper σ_{scat} and σ_{abs} values represent measurements taken at 550 nm and 528 nm, respectively. The TAP is a new instrument that uses the same operating principle as the Particle Soot Absorption Photometer (PSAP) and the same filters (47 mm PALL E70-2075W). Unlike the PSAP, the TAP rotates through 8 filter spots per individual filter along with two reference spots. During deployment at MBO, the TAP was set to rotate to the next filter spot when a filter spot's transmission reached 50%. The absorption coefficients were corrected using the filter loading and aerosol scattering correction factors derived for the 3λ PSAP by *Virkkula* [2010]. Uncertainty calculations were based on those used in a previous study at MBO for measurements with a 3λ PSAP [*Fischer et al.*, 2010a]. Sources of uncertainty include noise, instrument drift, errors in the loading function, the correction for the scattering artifact, and uncertainty in the flow and spot size corrections [*Anderson et al.*, 1999; *Bond et al.*, 1999; *Virkkula et al.*, 2005]. Combining these uncertainties yielded total uncertainties of ~25-40% during BB events.

Single scattering albedo (ω) for each event was calculated as the Reduced Major Axis (RMA) regression of scattering and total extinction (scattering + absorption) coefficient at 528 nm. To adjust the σ_{scat} value from 550 nm to 528 nm, a power law relationship was assumed

Formatted: Font: Not Italic
Formatted: Font color: Auto
Formatted: Font color: Auto
Formatted: Font color: Auto, Not Highlight
Formatted: Font color: Auto, Not Highlight
Formatted: Font color: Auto, Not Highlight
Formatted: Font: Bold, Font color: Auto, Not Highlight
Formatted: Font color: Auto, Not Highlight
Formatted: Font color: Auto, Not Highlight
Formatted: Font color: Auto, Not Highlight
Formatted: Font: Bold, Font color: Auto, Not Highlight
Formatted: Font color: Auto, Not Highlight
Formatted: Font color: Auto, Not Highlight
Formatted: Font color: Auto, Not Highlight
Formatted: Font: Bold, Font color: Auto, Not Highlight
Formatted: Font color: Auto, Not Highlight
Formatted: Font color: Auto
Formatted: Font color: Auto, Not Highlight
Formatted: Font color: Auto
Formatted: Font color: Auto, Not Highlight
Formatted: Font: Not Italic
Formatted: Font color: Auto

between scattering and wavelength. The 450-550 nm pair was used to adjust the 550 nm σ_{scat} measurement to 528 nm using ~~the~~ equation (1)~~:~~:

$$\sigma_{scat}^{528} = \sigma_{scat}^{550} * \left(\frac{\lambda_{550}}{\lambda_{528}}\right)^{SAE_{450,550}} \quad (1)$$

~~,~~where λ is wavelength and SAE is the scattering Ångström exponent calculated with the two wavelengths specified. The SAE values were calculated for each ~~sample~~5-minute interval using the scattering ~~coeficients~~coefficients measured at 450 nm and 550 nm. ~~-~~Mean SAE values for the BB plumes ranged from 1.61 to 2.15. Uncertainties for ω were calculated the same as the enhancement ratios, which is discussed in Section 2.4.

Absorption Ångström exponent (AAE) values were calculated for the absorption coefficient pair of 467 and 660 nm using equation (2) ~~[*Fischer et al.*, 2010a]~~:

$$AAE = -log(\sigma_{abs}^{467}/\sigma_{abs}^{660})/log(467/660) \quad (2)$$

~~-~~Uncertainties for AAE values were calculated by propagating the uncertainties from the measurements used to calculate AAE using addition in quadrature ~~as per~~ [*Fischer et al.*, 2010a].

We measured 5-minute averaged dry aerosol number size distribution with a TSI 3938 Scanning Mobility Particle Sizer (SMPS). The SMPS system consisted of a TSI 3082 electrostatic classifier with a TSI 3081 Differential Mobility Analyzer (DMA) and a TSI 3787 water-based condensation particle counter. A total of 107 bins were used to measure a diameter range from 14.1-637.8 nm. A sheath to aerosol flow ratio of 10:1 was used for the DMA. A multiple charge correction and diffusion loss correction were applied to the SMPS particle number concentration data using the TSI software. An additional diffusion correction for the inlet tube (15 m, 12 LPM) was applied assuming a laminar flow [*Hinds*, 1999]. Prior to deployment we confirmed the sizing accuracy of the SMPS using polystyrene latex spheres (PSL).

We measured dry particle mass under 1 µm (PM1) with an Optical Particle Counter (OPC, model 1.109, Grimm Technologies, Douglasville, GA). This is a U.S. EPA equivalent method for measuring PM2.5 mass concentration. The OPC was factory calibrated prior to deployment.

All particle measurements (σ_{scat}, σ_{abs}, PM1, number size distribution) were corrected to standard temperature and pressure (STP; T = 273.15, P = 101.325 kPa).

Formatted: Right
Formatted: Indent: First line: 0"
Formatted: Left, Indent: First line: 0"
Field Code Changed
Formatted: Justified, Indent: First line: 0"
Formatted: Font: Font color: Auto
Formatted: Font: Times New Roman, 12 pt
Formatted: Font: Times New Roman, 12 pt
Formatted: Font color: Auto
Formatted: Indent: First line: 0"
Formatted: Font color: Auto
Formatted: Not Highlight
Formatted: Font color: Auto
Field Code Changed
Formatted: Font: Font color: Black
Formatted: Font: Not Italic

2.4. Enhancement Ratio Calculations

Enhancement ratios (ΔY/ΔX) were calculated from the slope of the RMA regression of Y plotted against X. *Briggs et al.* [2016] calculated enhancement ratios (ERs) of BB plumes using three different methods, one method using the RMA slope of the linear correlation of two species, and two others calculating absolute enhancement above local background using two different definitions of background. All three methods produced similar results for $\Delta\sigma_{scat}/\Delta CO$, $\Delta NO_y/\Delta CO$, and PAN/ΔCO, but differing results for $\Delta O_3/\Delta CO$. In our study we used the RMA regression method for calculating ERs of $\Delta\sigma_{scat}/\Delta CO$ and ~~and~~ $\Delta\sigma_{abs}/\Delta CO$.~~.~~

Mass scattering and mass absorption efficiencies (MSE and MAE) were calculated as the enhancement ratios of $\Delta\sigma_{scat}/\Delta PM1$ and $\Delta\sigma_{abs}/\Delta PM1$, respectively, at 550 nm for σ_{scat} and 528 nm for σ_{abs}. As previously mentioned, ω was calculated as the RMA regression of scattering and total extinction (scattering + absorption). In all cases the enhancements (Δ) are large compared to background, thus avoiding the problems described by *Briggs et al.* [2016] for small enhancements above background.

We determined the uncertainties for the enhancement ratio calculations from the uncertainties in the extensive properties used in calculating the enhancement ratios and the uncertainty of the RMA regression using addition in quadrature. For example, the uncertainty in ΔX/ΔY was calculated by adding in quadrature the uncertainty in the RMA regression, the uncertainty in the X measurement, and the uncertainty in the Y measurement.

We present both precision uncertainty and total uncertainty as described by [*Anderson et al.*, 1999] for all values derived from optical measurements. Precision uncertainty includes uncertainty associated with noise and instrument drift. This is best used when comparing measurements collected using the same instruments and protocols. It is the appropriate uncertainty to consider when comparing individual BB events seen at MBO in this study. Total uncertainty includes precision uncertainty, the uncertainty associated with the corrections we applied to the data, and the uncertainty associated with the calibration method. This is the appropriate uncertainty to consider when comparing the measurements presented in this study with data collected using other measurement methods.

2.5. Biomass Burning Event Identification

Formatted: Font: Not Italic

Formatted: Not Highlight

We identified BB events as time periods during which 5-min ambient aerosol scattering coefficients σ_{scat} > 20 Mm^{-1} for at least one hour, 5-min CO > 150 ppbv for at least one hour, and there was~~is~~ a strong correlation (R^2 > 0.80) between σ_{scat} and CO. To determine fire locations we calculated back-trajectories using the National Oceanic and Atmospheric Administration Hybrid Single-Particle Lagrangian Integrated Trajectory (HYSPLIT) model, version 4 [*Draxler*, 1999; *Draxler and Hess*, 1997; 1998; *Stein et al.*, 2015]. We used the Global Data Assimilation System (GDAS) 1° × 1° gridded meteorological data from the National Oceanographic and Atmospheric Administration's Air Resources Laboratory (NOAA-ARL). Within GDAS, the grid containing MBO is located at ~1500 m amgl (above model ground level) so back-trajectory starting heights of 1300, 1500, and 1700 m amgl were chosen [*Ambrose et al.*, 2011]. We identified fire locations using Moderate Resolution Imaging Spectroradiometer (MODIS) satellite-derived active fire counts [*Justice et al.*, 2002], and Fire INventory from NCAR (FINN) data [*Wiedinmyer et al., 2011*]. ~~-~~Similar criteria for identifying BB events has been used by *Baylon et al.* [2015] and *Wigder et al.* [2013] from data collected at MBO.

Formatted: Font: Not Italic

Field Code Changed

Formatted: Font: Not Italic

Formatted: Font: Not Italic

3. Results and Discussion

3.1. Identified BB ~~events~~ Events and Fire Source Identification

The summer of 2015 was a very active fire season in the Pacific Northwest~~West~~ (Figure 1). During the month of August 2015, 51% of the 5~~-~~-minute averages met the criteria for a BB event, ~~of~~ having σ_{scat} > 20 Mm^{-1} and CO > 150 ppbv, including several multi-day periods. We split these multi-day events up if discernable plumes within the event could be identified. Altogether we identified 19 events, ranging from 1.5-45 hours in duration. We use the term *event*, not *plume*, because of the long duration of some of the events and the fact that most BB events observed in 2015 were influenced by emissions from multiple fires.

Formatted: Font: Italic

Formatted: Font: Italic

Two large multi-day events of regional BB smoke from fires in Northern California and Southwestern Oregon dominated the sampling period (dotted boxes in Figure 2). ~~We categorized most of the events into three main periods (Figure 2). Periods 1 (8/9/15-8/12/15: events 2-8) and 3 (8/23/15-8/29/15: events 16-19) are both multi-day periods that experienced regional BB smoke from fires in Northern California and Southwestern Oregon.~~ Transport time from these regional fires to MBO, estimated from the back-trajectories, ranged from 3-3~~0~~ hours. In

between these two large regional BB events there was a time period that was influenced by Siberian wildfires (solid box in Figure 2). ~~Period 3 2 (8/17/15-8/22/15: events 10-15) is characterized by influence from Siberian BB events.~~ During August there were intense forest fires around Lake Baikal in Siberia, peaking on 8/8/2015 with a total fire area of 681 km^2, and an estimated CO and BC emissions of $3.22x10^8$ and $1.33x10^6$ kg/day, respectively (*Fire INventory from NCAR (FINN) data) [Wiedinmyer et al., 2011]*. Transport times from ~~the N~~northeastern Asia to MBO during these events ranged from 4-10 days. NASA MODIS aqua and terra images show the eastward transport of smoke from the Lake Baikal fires during this time period [*https://worldview.earthdata.nasa.gov/*, 2016]. We used V3.30 aerosol classification products from the Cloud-Aerosol Lidar with Orthogonal Polarization (CALIOP) instrument on the Cloud-Aerosol Lidar Infrared Pathfinder Satellite Observation (CALIPSO) satellite to confirm the transport of plumes of smoke from the Siberian fires to North America [*http://www-calipso.larc.nasa.gov/*, 2016; *Winker et al.*, 2010; *Winker et al.*, 2009]. Aerosol plumes are identified as one of six types: dust, polluted continental, polluted dust, smoke (biomass burning), clean continental or clean marine aerosols [*Omar et al.*, 2009].

3.2. Overview of Summer 2015 BB Events ~~from difference sources~~

Table 1 provides an overview of the 19 BB events from MBO during the summer of 2015. We calculated water vapor enhancement (ΔWV) to indicate the origin of the event air mass. Positive ΔWV suggest the air mass ascended from the boundary layer (BL) to MBO, ~~to~~ while near zero or negative values mean the air mass is relatively dry and likely descended or arrived from the free troposphere (FT) [*Baylon et al.*, 2015; *Wigder et al.*, 2013]. All of the regional BB events have ΔWV values ≥ 1.00 g/kg, while all of the Siberian-influenced events have ΔWV values near zero or negative. The precision and total uncertainties for all of the parameters derived from optical measurements are provided for these events in Table S1.

We found the $\Delta\sigma_{scat}/\Delta CO$ (σ_{scat} at STP) enhancement ratio to range from 0.48-1.29 Mm^{-1} ~~/~~ppbv^{-1}, with the majority of events being between 0.8 and 1.25 Mm^{-1} ~~/~~ppbv^{-1}. We found ΔPM1/ΔCO (PM1 at STP) to range from 0.18-0.43 μg cm^{-3} ~~/~~ppbv^{-1}. These values are in the same range as BB plumes seen previously at MBO [*Baylon et al.*, 2015; *Wigder et al.*, 2013].

In 2015 many fires were burning throughout the northwestern U.S. So in contrast to previous work at MBO, we were not able to calculate transport time for any of the regional BB

Formatted: Superscript
Formatted: Superscript
Formatted: Superscript
Field Code Changed
Formatted: Font color: Auto
Formatted: Font color: Auto

events observed as they were influenced by multiple fires with various transport times. Figure 3 provides an example of this and exemplifies the impossibility of determining an exact transport time.

3.3. Optical Properties of the BB Aerosol at MBO

We observed significant differences in the optical properties of regional and Siberian-influenced BB events. The Siberian-influenced events had ~~enhanced~~ higher absorption coefficients relative to other measurements ~~made~~. This resulted in higher $\Delta\sigma_{abs}/\Delta CO$, higher MAE ($\Delta\sigma_{abs}/\Delta PM1$), and lower ω ($\sigma_{scat}/(\sigma_{scat} + \sigma_{abs})$) compared to regional BB events (Figures ~~4~~3 and ~~5~~4). We found no significant differences for $\Delta\sigma_{scat}/\Delta CO$ or MSE ($\Delta\sigma_{scat}/\Delta PM1$) between regional and Siberian events. ~~Event 9 was anomalous in that it has very low absorption enhancement, a high ω, and is not part of the designated Periods defined in section 3.1. Back-trajectories show that event 9 came from the boundary layer under stagnant conditions, indicating an aged and mixed source.~~ Back-trajectories for the Siberian events (events 10-15) originated at high elevation over Siberia, suggesting that the BB emissions~~)~~ were lofted to altitudes of~~indicate that the plumes were lofted to altitudes of~~ 4-10 km (Figure ~~S1~~6). The Siberian events at MBO were observed over the course of a week (8/17/2015-8/23/2015)~~:,~~ therefore the back-trajectories in ~~Fig. S1~~Figure 6 represent a sustained meteorological pattern that consistently transported Siberian smoke to North America throughout the week. Aerosol vertical profiles measured by CALIOP corroborate the transport of BB plumes from the Siberian fires across the Pacific at altitudes of 4-10 km. Large BB plumes were identified over Northeast Asian and the North Pacific consisting primarily of BB smoke and some polluted dust over the Northern Pacific from 8/8/2015-8/17/2015. Figures S~~2~~1-~~S5~~ S4 show selected CALIPSO transects from 8/13/2015-8/16/2015 over the Pacific. The location and altitude of these plumes match the back-trajectories calculated from MBO for the Siberian events (Figure 6~~S1~~), verifying that events 10-15 are heavily influenced by the Siberian fires.

We ~~theorize~~ suggest that the Siberian BB events observed at MBO represent hotter, more flaming portions of the fires which have higher BC emissions and thus higher absorption enhancements compared to the regional BB events. ~~-~~The hotter parts of the fires have more pyro-convective energy to loft the plume high into the atmosphere where it can then undergo long-range transport. During the ARCTAS-A flight campaign in Alaska, Siberian fire plumes were found to have a much larger BC/CO ratio (8.5 ± 5.4 ng m^{-3} /ppbv^{-1}) than North American fire

Formatted: Font: Times New Roman, Font color: Auto

Formatted: Superscript

Formatted: Superscript

plumes (2.3 ± 2.2 ng m^{-3}/ ppbv^{-1}) [*Kondo et al.*, 2011]. This difference was attributed to the Siberian fires having a higher modified combustion efficiency (MCE). In addition, for the Siberian BB plumes they found MCE to increase with altitude. *Jolleys et al.* [2015] correspondingly found higher ΔBC/ΔOA (Δblack carbon/Δorganic aerosol) ratios to increase with altitude in eEastern Canadian BB plumes. Intense, flaming fire plumes have higher injection heights into the atmosphere due to enhanced pyro-convection, whereas smoldering fires have low thermal convective energy and are mostly contained within the boundary layer. BB aerosol lofted to the free troposphere via pyro-convection is less likely to be removed and can have a longer atmospheric lifetime of up to 40 days [*Bond et al.*, 2013]. The back-trajectories for the Siberian events corroborate this idea. They were all relatively dry (water vapor mixing ratio < 5 g kg^{-1}) with little precipitation during transport, suggesting the aerosol in the Siberian events was subjected to very limited wet deposition, which is the main removal mechanism from the atmosphere. Flaming conditions produce more ~~black carbon (~~BC~~)~~ and less ~~organic aerosol (~~OA~~)~~ generally, which leads to amplified absorption [*Vakkari et al.*, 2014; *Yokelson et al.*, 2009]. Flaming conditions are associated with high ~~modified combustion efficiency (~~MCE~~)~~ values [*Reid et al.*, 2005a]. Unfortunately, we were not able to calculate MCE values for the Siberian events at MBO due to extensive dilution and boundary layer mixing during transport [*Yokelson et al.*, 2013a].

While the ω values for the Siberian events are significantly lower relative to the regional events, they are all high (> 0.95) compared to typical flaming conditions measured in the laboratory or near-field measurements [*S Liu et al.*, 2014a; *Vakkari et al.*, 2014]. *S Liu et al.* [2014a] found a robust relationship between ω and MCE in laboratory BB emissions where MCE was negatively correlated with ω. However, observations have found that ω increases significantly after emission in BB plumes [*Reid et al.*, 2005a; *Vakkari et al.*, 2014]. A previous study at MBO found that well-aged BB plumes do not follow the *S Liu et al.* [2014a] parametrization [*Briggs et al.*, 2016]. All of the BB plumes observed by *Briggs et al.* [2016] had ω>0.91 despite MCE values as high as 0.98, and no relationship was found between ω and MCE. The high ω values typical of aged BB plumes are most likely due to SOA formation and increased scattering efficiency as the particles ages and increases in size through coagulation and condensation. Given this we believe the ω's seen in these Siberian plumes are different and

Formatted: Superscript
Formatted: Superscript
Formatted: Superscript
Field Code Changed
Field Code Changed
Field Code Changed

significantly higher than the ω's directly after emission and are therefore cannot be equated to an MCE value.

We found AAE values for the Siberian events to be significantly lower than regional BB events (Figures ~~3~~ 4 and ~~4~~5). High AAE values are indicative of the presence of brown carbon (BrC). Brown carbon is a fraction of ~~organic aerosol (~~OA~~)~~ that selectively absorbs short wavelengths [*Andreae and Gelencser*, 2006; *Chen and Bond*, 2010; *Kirchstetter et al.*, 2004]. There are two possible explanations for the difference in AAE values. The first is that the flaming conditions that produced the Siberian events seen at MBO had higher BC and lower OA emissions, which inherently have lower AAE as total absorption is dominated by BC and ~~there is less~~less BrC is ~~in the aeroso~~initially produced~~l~~. Laboratory and field studies have corroborated this and observed an inverse relationship between MCE and AAE [*Holder et al.*, 2016; *S Liu et al.*, 2014a; *McMeeking et al.*, 2014]. The other explanation is that BrC is lost during transport through photobleaching, volatilization, and aerosol-phase reactions. *Forrister et al.* [2015] determined that BrC decreased with transport with a half-life of 9 hours and that AAE decreases from ~4.0 to ~2.5 24 hours after emission. All of the regional BB events ~~(Periods 1 and 3)~~ were influenced by multiple fires that had transport times varying from 3- ~~30~~ 35 hours. With each event being influenced by at least one fire with a transport time ≤ 6 hours, this short transport time is consistent with the higher AAE values we observed.

3.4. Mass Scattering Efficiency

Mass scattering efficiencies (MSEs) are important for calculating the radiative forcing effects of aerosols in global climate and chemical transport models. Estimates of MSE are used to convert aerosol mass measurements to aerosol optical properties [*Briggs et al.*, 2016; *Hand and Malm*, 2007; *Pitchford et al.*, 2007]. MSE is dependent on particle composition, which determines the particle's refractive index and hygroscopicity~~hygroscopy~~, and aerosol size distribution [*Hand and Malm*, 2007]. We calculated MSE~~'s~~ as the slope of the RMA regression of σ_{scat} and PM1 ($\Delta\sigma_{scat}/\Delta PM1$). R^2 values were >0.94 for all events. We found MSE values ~~to~~ ranged from 2.50-4.76 $m^2\ g^{-1}$, which are consistent with previously measured values.

Formatted: Font: Not Italic

During 2013 at MBO, MSE values estimated using AMS organic matter (OM) data and the σ_{scat} for four wildfire plumes ranged from 2.8-4.8 $m^2\ g^{-1}$ (mean: 3.7 $m^2\ g^{-1}$) [*Briggs et al.*, 2016]. *Levin et al.* [2010] calculated MSE values for fresh BB smoke from a variety of fuels to

range from 1.5–5.7 m^2 g^{-1}, with most of the values falling between 2.0 and 4.5 m^2 g^{-1}. *Reid et al.* [2005a] reviewed MSE values from BB events and found a range between 3.2 and 4.2 m^2 g^{-1} (mean: 3.8 m^2 g^{-1}) for temperate and boreal fresh smoke, and larger values for aged smoke (3.5-4.6 m^2 g^{-1}; mean: 4.3 m^2 g^{-1}). MSE values upwards of ~6 m^2 g^{-1} have been observed for aged BB plumes [*Hand and Malm*, 2007; *McMeeking et al.*, 2005]. Due to the large variation in MSE values for BB events, assigning an average MSE value to convert aerosol mass measurements to aerosol optical properties or vice versa introduces significant uncertainties.

We investigated the cause for the variation in the MSE values that we observed ~~(Figure S5)~~. We found MSE's for BB events to be positively correlated with D_{pm} (R^2 = 0.73) (Figure ~~5A~~S~~7~~5a). ~~-~~If two D_{pm} values associated with bimodal size distributions are removed, the correlation increases substantially (R^2 = 0.88). A positive correlation between MSE and mean particle diameter has previously been observed in ambient data [*Lowenthal and Kumar*, 2004] and laboratory studies [*McMeeking et al.*, 2005]. Theoretically according to M~~ei~~ie theory, MSE will increases as the average particle diameter grows, through coagulation and condensation, toward the measurement wavelength (550 nm) [*Seinfeld and Pandis*, 2006].

~~MSE was also well correlated with event integrated σ_{scat} (R^2 = 0.90) and PM1 mass (R^2 = 0.85), and slightly correlated with CO (R^2 = 0.53) (Figure 5b,c,d). The dependence of MSE on mass concentration [*Malm and Hand*, 2007] and σ_{scat} [*Lowenthal and Kumar*, 2004] has previously been observed, although it is mainly thought to be a function of particle size.~~

3.5. BB Size Distributions

Figure ~~8~~6 shows the BB aerosol number size distributions for the events we observed at MBO in dN/dlogDp ~~(Figure 6)~~. We found D_{pm} and σ_g of the number distributions to range from 138-229 nm and 1.53-1.89, respectively. The size distributions observed at MBO are similar to *Janhäll et al.* [2010], who compiled aged ~~biomass burning~~BB size distributions. They found the accumulation mode mean diameter to range from 175~~–~~300 nm with geometric standard deviations of 1.3–1.7. No dependence was found in D_{pm} in plumes of regional or Siberian origins. Similarly d~~D~~uring the ARCTAS-B flight campaign, aged BB plumes of ~~Western~~ western Canadian and Asian origins were found to have similar size distributions (Canadian: D_{pm} = 224 ±

Formatted: Font color: Red
Formatted: Font color: Auto, Not Highlight
Field Code Changed
Field Code Changed
Field Code Changed
Formatted: Highlight
Formatted: Superscript
Formatted: Highlight
Formatted: Highlight
Formatted: Highlight
Formatted: Add space between paragraphs of the same style, Line spacing: 1.5 lines
Formatted: Subscript

14 nm, σ_g = 1.31 ± 0.05; Asian: D_{pm} = 238 ± 11 nm, σ_g = 1.31 ± 0.03) [*Kondo et al.*, 2011]. The BORTAS-B flight campaign in Eastern Canada observed aged BB plumes with median diameters of 180-240 nm [*Sakamoto et al.*, 2015].

We observed clear bimodal distributions with an accumulation mode (100-500 nm) and Aitken mode (20-100 nm) for five events (2, 3, 11, 14 and 15). The Aitken mode in these size distributions most likely represents a secondary source from within the boundary layer. A prominent "tail" consisting of higher than expected number concentrations of small-diameter particles (30-90 nm) was observed for most of the unimodal events at MBO. It would be expected that particles in this size range would grow to larger particles through coagulation relatively quickly. *Sakamoto et al.* [2015] observed a similar elevation in the number concentration of small particles during the BORTAS-B campaign. They attempted to account for the existence of the tail with a Lagrangian box model of coagulation and dilution but were unable to do so. Coagulation should cause a significant decrease in Aitken mode particles in a matter of hours; and nucleation and condensation growth rates would have to be unreasonably high to maintain these small particles.

We observed no clear distinction between the size distributions from regional and Siberian events. These results are consistent with previous studies that have not observed a dependence from plume age, transport time, or source location on the BB size distribution. *Kondo et al.* [2011] found little difference between the D_{pm} of Siberian and Canadian BB plumes despite different chemical composition, ~~and~~ optical properties, and transport times. Similarly, *Sakamoto et al.* [2015] found no trend in size distribution with plume transport distance. In a study performed in the Front Range of Colorado, *Carrico et al.* [2016] found no significant difference between the size distribution of an hours old and a days old fire plume.

As previously stated, we found MSE's for BB events to be positively correlated with D_{pm}. This makes physical sense due to increased light scattering efficiency of larger particles closer to the wavelength of light (550 nm). In addition, we found ~~We also found~~ ~~We found~~ event integrated D_{pm} to be correlated with event integrated σ_{scat} (R^2 = 0.65) and PM1 mass (R^2 = 0.72), and moderately correlated with CO (R^2 = 0.41~~0~~) (Figure 7b,c,d). D_{pm} was not found to be correlated with any normalized enhancement ratio ($\Delta\sigma_{scat}/\Delta CO$, $\Delta PM1/\Delta CO$). CO, σ_{scat}, and PM1 can be thought of as surrogates for plume concentration. The

Formatted: Font color: Auto

correlation between these proxies of plume concentration and D_{pm} in ~~Therefore~~ ~~This in~~dicates that~~,~~ in general, the more concentrated ~~the~~ BB plumes have ~~, the l~~larger size distributions.

In a related study, *Sakamoto et al.* [2016] ~~*Sakamoto et al.* [In Press], we~~ selected subsets of the MBO BB regional events presented here and tested them against parameterizations of the aged size distribution. The parameterizations calculate D_{pm} and σ_g from inputs that can be derived from emissions-inventory and meteorological parameters. The seven inputs are: emission median dry diameter, emission distribution modal width, mass emissions flux, fire area, mean boundary-layer wind speed, plume mixing depth, and time/distance since emission. We identified eleven plumes from regional events that had consistent transport to known regional fires. The simple fits captured over half of the variability in observed D_{pm} and modal width, even though the freshly emitted D_{pm} and modal widths were unknown. The results demonstrate that the parameterizations presented in *Sakamoto et al.* [2016] ~~*Sakamoto et al.* [In Press]~~ section 3.4 can be successfully used to estimate aged BB size distributions in regional BB plumes with transport times up to 35 hours. Using these parameterizations to estimate BB plume size distribution in global and regional aerosol models is a significant improvement to assuming fixed values for size-distribution parameters.

~~In a previous study,~~ The *Sakamoto et al.* [2016] ~~, coagulation only~~ parameterizations ~~for effective biomass burning size distributions (D_{pm} and σ_g) were developed from inputs that can be derived from emissions inventory and meteorological parameters. The seven inputs are: emission median dry diameter, emission distribution modal width, mass emissions flux, fire area, mean boundary layer wind speed, plume mixing depth, and time/distance since emission. The size distribution.~~ ~~was~~were particularly sensitive to mass emissions flux and~~,~~ fire area, as well as wind speed and transport time. If mass emissions flux is interpreted as surrogate for plume concentration, this agrees with our conclusion that increased plume concentration results in a larger size distribution.

4. ~~—~~Conclusions

We characterized the physical and optical properties of 19 aged biomass burning events observed at the Mt. Bachelor Observatory in the summer of 2015. Regional (Northern California and Southwestern Oregon) and Siberian events were observed. Our main conclusions were:

Formatted: Subscript, Not Highlight

Formatted: Font color: Auto

Field Code Changed

Formatted: Font color: Auto

Formatted: Not Highlight

Formatted: Not Highlight

Formatted: Font: Bold

Formatted: Space Before: 12 pt, After: 12 pt, Line spacing: single

- $\Delta\sigma_{scat}/\Delta CO$ (σ_{scat} at STP) enhancement ratio ~~to~~ ranged from 0.48-1.29 Mm^{-1}~~/~~ $ppbv^{-1}$~~,~~, with the majority of events being between 0.8 and 1.25 Mm^{-1} $ppbv^{-1}$~~Mm^{-1}/ppbv~~.

- Siberian-influenced events had significantly higher $\Delta\sigma_{abs}/\Delta CO$ and MAE, and lower ω compared to regional events. We propose this is due to MBO sampling the portion on Siberian smoke that has been lofted to higher elevation through pyro-convection~~.~~, thereby preferentially sampling emissions of strong flaming combustion conditions. In general flaming conditions produce more BC, which would explain the amplified absorption in the Siberian events.

- Absorption Ångström exponent values were significantly lower for the Siberian events than regional events, which indicates lack of BrC produced by the Siberian fires or loss of BrC during transport through photobleaching, volatilization, and aerosol-phase reactions.

- Mass scattering efficiencies ranged from 2.50-4.76 m^2 g^{-1}. MSE was positively correlated with D_{pm} (R^2 = 0.73), which agrees with Mie T~~t~~heory.

- Aerosol number size distribution D_{pm} and σ_g ranged from 138-229 nm and 1.53-1.89, respectively. Five of the nineteen events had bimodal distributions, the rest being unimodal. The unimodal distributions had a prominent "tail" of small-diameter particles (30-90 nm). No distinction could be made between regional and Siberian size distributions.

Formatted: Superscript

4. Author Contribution

J~~.~~ames R. Laing ~~preformed~~ performed the data analysis and prepared the manuscript with assistance from all co-authors.

5. Acknowledgments

Funding for research at MBO was supported by the National Science Foundation (grant number: 1447832). ~~The~~ MBO is also supported by a grant from the NOAA Earth System Research Laboratory. The views, opinions and findings contained in this report are those of the author(s) and should not be construed as an official National Oceanic and Atmospheric Administration or U.S. Government position, policy or decision. The authors gratefully acknowledge the NOAA Air Resources Laboratory (ARL) for the provision of the HYSPLIT

transport model used in this publication. The CALIPSO satellite products ~~was~~ were supplied from the NASA Langley Research Center.

References:

Akagi, S. K., et al. (2012), Evolution of trace gases and particles emitted by a chaparral fire in California, *Atmospheric Chemistry and Physics*, *12*, 1397-1421, doi:10.5194/acp-12-1397-2012.

Ambrose, J. L., D. R. Reidmiller, and D. A. Jaffe (2011), Causes of high O(3) in the lower free troposphere over the Pacific Northwest as observed at the Mt. Bachelor Observatory, *Atmospheric Environment*, *45*, 5302-5315, doi:10.1016/j.atmosenv.2011.06.056.

Anderson, T. L., D. Covert, J. Wheeler, J. Harris, K. Perry, B. Trost, D. Jaffe, and J. Ogren (1999), Aerosol backscatter fraction and single scattering albedo: Measured values and uncertainties at a coastal station in the Pacific Northwest, *J. Geophys. Res.*, *104*(D21), 26793-26807.

Anderson, T. L., and J. A. Ogren (1998), Determining aerosol radiative properties using the TSI 3563 integrating nephelometer, *Aerosol Science and Technology*, *29*(1), 57-69.

Andreae, M. O., and A. Gelencser (2006), Black carbon or brown carbon? The nature of light-absorbing carbonaceous aerosols, *Atmospheric Chemistry and Physics*, *6*, 3131-3148.

Andreae, M. O., and P. Merlet (2001), Emission of trace gases and aerosols from biomass burning, *Global Biogeochemical Cycles*, *15*, 955-966, doi:10.1029/2000gb001382.

Baylon, P., D. A. Jaffe, N. L. Wigder, H. Gao, and J. Hee (2015), Ozone enhancement in western US wildfire plumes at the Mt. Bachelor Observatory: The role of NOx, *Atmospheric Environment*, *109*, 297-304, doi:http://dx.doi.org/10.1016/j.atmosenv.2014.09.013.

Bond, T. C., T. L. Anderson, and D. Campbell (1999), Calibration and intercomparison of filter-based measurements of visible light absorption by aerosols, *Aerosol Science & Technology*, *30*(6), 582-600.

Bond, T. C., et al. (2013), Bounding the role of black carbon in the climate system: A scientific assessment, *J. Geophys. Res.*, *118*, 1-173, doi:10.1002/jgrd.50171.

Bond, T. C., D. G. Streets, K. F. Yarber, S. M. Nelson, J. H. Woo, and Z. Klimont (2004), A technology-based global inventory of black and organic carbon emissions from combustion, *Journal of Geophysical Research-Atmospheres*, *109*(D14), 43, doi:10.1029/2003jd003697.

Boucher, O., et al. (2013), Clouds and Aerosols, in *Climate Change 2013: The Physical Science Basis. Contribution of Working Group I to the Fifth Assessment Report of the Intergovernmental Panel on Climate Change*, edited by T. F. Stocker, D. Qin, G.-K. Plattner, M. Tignor, S. K. Allen, J. Boschung, A. Nauels, Y. Xia, V. Bex and P. M. Midgley, Cambridge University Press, Cambridge, UK.

Briggs, N. L., D. A. Jaffe, H. Gao, J. R. Hee, P. M. Baylon, Q. Zhang, S. Zhou, S. C. Collier, P. D. Sampson, and R. A. Cary (2016), Particulate Matter, Ozone, and Nitrogen Species in Aged Wildfire Plumes Observed at the Mount Bachelor Observatory.

Carrico, C. M., A. J. Prenni, S. M. Kreidenweis, E. J. Levin, C. S. McCluskey, P. J. DeMott, G. R. McMeeking, S. Nakao, C. Stockwell, and R. J. Yokelson (2016), Rapidly evolving ultrafine and fine mode biomass smoke physical properties: Comparing laboratory and field results, *J. Geophys. Res.*

Chen, Y., and T. C. Bond (2010), Light absorption by organic carbon from wood combustion, *Atmospheric Chemistry and Physics*, *10*(4), 1773-1787.

Collier, S., S. Zhou, T. B. Onasch, D. A. Jaffe, L. Kleinman, A. J. Sedlacek III, N. L. Briggs, J. Hee, E. Fortner, and J. E. Shilling (2016), Regional Influence of Aerosol Emissions from Wildfires Driven by Combustion Efficiency: Insights from the BBOP Campaign, *Environmental Science & Technology*, *50*(16), 8613-8622.
Draxler, R. R. (1999), HYSPLIT4 user's guide, NOAA Tech. Memo*Rep.*, NOAA Air Resources Laboratory, Silver Spring, MD.
Draxler, R. R., and G. D. Hess (1997), Description of the HYSPLIT_4 modeling system, NOAA Tech. Memo*Rep.*, 24 pp, NOAA Air Resources Laboratory, Silver Spring, MD.
Draxler, R. R., and G. D. Hess (1998), An overview of the HYSPLIT_4 modeling system of trajectories, dispersion, and deposition, *Australian Meteorological Magazine*, *47*, 295-308.
Fischer, E. V., D. A. Jaffe, N. A. Marley, J. S. Gaffney, and A. Marchany-Rivera (2010a), Optical properties of aged Asian aerosols observed over the US Pacific Northwest, *Journal of Geophysical Research-Atmospheres*, *115*, D20209-D20209, doi:10.1029/2010JD013943.
Fischer, E. V., D. A. Jaffe, D. R. Reidmiller, and L. Jaeglé (2010b), Meteorological controls on observed peroxyacetyl nitrate at Mount Bachelor during the spring of 2008, *Journal of Geophysical Research*, *115*, D03302, doi:10.1029/2009jd012776.
Flannigan, M. D., M. A. Krawchuk, W. J. de Groot, B. M. Wotton, and L. M. Gowman (2009), Implications of changing climate for global wildland fire, *Int J Wildland Fire*, *18*(5), 483-507.
Forrister, H., J. Liu, E. Scheuer, J. Dibb, L. Ziemba, K. L. Thornhill, B. Anderson, G. Diskin, A. E. Perring, and J. P. Schwarz (2015), Evolution of brown carbon in wildfire plumes, *Geophysical Research Letters*, *42*(11), 4623-4630.
Gratz, L. E., D. A. Jaffe, and J. R. Hee (2014), Causes of increasing ozone and decreasing carbon monoxide in springtime at the Mt. Bachelor Observatory from 2004 to 2013, *Atmospheric Environment*, doi:10.1016/j.atmosenv.2014.05.076.
Hand, J. L., and W. C. Malm (2007), Review of aerosol mass scattering efficiencies from ground-based measurements since 1990, *Journal of Geophysical Research*, *112*, D16203, doi:10.1029/2007jd008484.
Haywood, J., and O. Boucher (2000), Estimates of the direct and indirect radiative forcing due to tropospheric aerosols: A review, *Reviews of Geophysics*, *38*(4), 513-543, doi:10.1029/1999rg000078.
Hinds, W. C. (1999), *Aerosol Technology: Properties, Behavior, and Measurement of Airborne Particles, 2nd Edition*, John Wiley & Sons, Inc., New York.
Hobbs, P. V. (2003), Evolution of gases and particles from a savanna fire in South Africa, *Journal of Geophysical Research*, *108*, doi:10.1029/2002jd002352.
Holder, A. L., G. S. Hagler, J. Aurell, M. D. Hays, and B. K. Gullett (2016), Particulate matter and black carbon optical properties and emission factors from prescribed fires in the southeastern United States, *J. Geophys. Res.*, *121*(7), 3465-3483.
Hosseini, S., Q. Li, D. Cocker, D. Weise, A. Miller, M. Shrivastava, J. W. Miller, S. Mahalingam, M. Princevac, and H. Jung (2010), Particle size distributions from laboratory-scale biomass fires using fast response instruments, *Atmospheric Chemistry and Physics*, *10*(16), 8065-8076, doi:10.5194/acp-10-8065-2010.
http://www-calipso.larc.nasa.gov/ (2016), NASA The Cloud-Aerosol Lidar and Infrared Pathfinder Satellite Observation (CALIPSO), edited.
https://worldview.earthdata.nasa.gov/ (2016), NASA WorldView.

Jaffe, D. A., E. Prestbo, P. Swartzendruber, P. Weiss-Penzias, S. Kato, A. Takami, S. Hatakeyama, and Y. Kajii (2005), Export of atmospheric mercury from Asia, *Atmospheric Environment*, *39*(17), 3029-3038, doi:10.1016/j.atmosenv.2005.01.030.

Janhäll, S., M. O. Andreae, and U. Pöschl (2010), Biomass burning aerosol emissions from vegetation fires: particle number and mass emission factors and size distributions, *Atmospheric Chemistry and Physics*, *10*(3), 1427-1439.

Jolleys, M. D., et al. (2015), Properties and evolution of biomass burning organic aerosol from Canadian boreal forest fires, *Atmospheric Chemistry and Physics*, *15*(6), 3077-3095, doi:10.5194/acp-15-3077-2015.

Justice, C. O., L. Giglio, S. Korontzi, J. Owens, J. T. Morisette, D. Roy, J. Descloitres, S. Alleaume, F. Petitcolin, and Y. Kaufman (2002), The MODIS fire products, *Remote Sensing of Environment*, *83*(1-2), 244-262, doi:10.1016/s0034-4257(02)00076-7.

Kirchstetter, T. W., T. Novakov, and P. V. Hobbs (2004), Evidence that the spectral dependence of light absorption by aerosols is affected by organic carbon, *Journal of Geophysical Research-Atmospheres*, *109*(D21), 12, doi:10.1029/2004jd004999.

Kondo, Y., et al. (2011), Emissions of black carbon, organic, and inorganic aerosols from biomass burning in North America and Asia in 2008, *Journal of Geophysical Research-Atmospheres*, *116*, 25, doi:10.1029/2010jd015152.

Levin, E. J. T., et al. (2010), Biomass burning smoke aerosol properties measured during Fire Laboratory at Missoula Experiments (FLAME), *Journal of Geophysical Research-Atmospheres*, *115*, 15, doi:10.1029/2009jd013601.

Liu, S., et al. (2014a), Aerosol single scattering albedo dependence on biomass combustion efficiency: Laboratory and field studies, *Geophysical Research Letters*, *41*(2), 742-748, doi:10.1002/2013gl058392.

Liu, Y., S. Goodrick, and W. Heilman (2014b), Wildland fire emissions, carbon, and climate: Wildfire-climate interactions, *Forest Ecology and Management*, *317*, 80-96, doi:10.1016/j.foreco.2013.02.020.

Lowenthal, D. H., and N. Kumar (2004), Variation of mass scattering efficiencies in IMPROVE, *Journal of the Air & Waste Management Association*, *54*(8), 926-934.

May, A. A., T. Lee, G. R. McMeeking, S. Akagi, A. P. Sullivan, S. Urbanski, R. J. Yokelson, and S. M. Kreidenweis (2015), Observations and analysis of organic aerosol evolution in some prescribed fire smoke plumes, *Atmospheric Chemistry and Physics*, *15*(11), 6323-6335, doi:10.5194/acp-15-6323-2015.

May, A. A., E. J. T. Levin, C. J. Hennigan, I. Riipinen, T. Lee, J. L. Collett, J. L. Jimenez, S. M. Kreidenweis, and A. L. Robinson (2013), Gas-particle partitioning of primary organic aerosol emissions: 3. Biomass burning, *Journal of Geophysical Research-Atmospheres*, *118*(19), 11327-11338, doi:10.1002/jgrd.50828.

May, A. A., et al. (2014), Aerosol emissions from prescribed fires in the United States: A synthesis of laboratory and aircraft measurements, *Journal of Geophysical Research-Atmospheres*, *119*(20), 11826-11849, doi:10.1002/2014jd021848.

McMeeking, G. R., E. Fortner, T. B. Onasch, J. W. Taylor, M. Flynn, H. Coe, and S. M. Kreidenweis (2014), Impacts of nonrefractory material on light absorption by aerosols emitted from biomass burning, *Journal of Geophysical Research-Atmospheres*, *119*, 12272-12286, doi:10.1002/2014jd021750.

McMeeking, G. R., S. M. Kreidenweis, C. M. Carrico, T. Lee, J. L. Collett, and W. C. Malm (2005), Observations of smoke-influenced aerosol during the Yosemite Aerosol Characterization

Study: Size distributions and chemical composition, *Journal of Geophysical Research-Atmospheres*, *110*(D9).
Okoshi, R., A. Rasheed, G. C. Reddy, C. J. McCrowey, and D. B. Curtis (2014), Size and mass distributions of ground-level sub-micrometer biomass burning aerosol from small wildfires, *Atmospheric Environment*, *89*, 392-402, doi:10.1016/j.atmosenv.2014.01.024.
Omar, A. H., D. M. Winker, M. A. Vaughan, Y. Hu, C. R. Trepte, R. A. Ferrare, K.-P. Lee, C. A. Hostetler, C. Kittaka, and R. R. Rogers (2009), The CALIPSO automated aerosol classification and lidar ratio selection algorithm, *Journal of Atmospheric and Oceanic Technology*, *26*(10), 1994-2014.
Pierce, J. R., K. Chen, and P. J. Adams (2007), Contribution of primary carbonaceous aerosol to cloud condensation nuclei: processes and uncertainties evaluated with a global aerosol microphysics model, *Atmospheric Chemistry and Physics*, *7*(20), 5447-5466.
Pitchford, M., W. Malm, B. Schichtel, N. Kumar, D. Lowenthal, and J. Hand (2007), Revised algorithm for estimating light extinction from IMPROVE particle speciation data, *Journal of the Air & Waste Management Association*, *57*(11), 1326-1336.
Reid, J. S., T. F. Eck, S. A. Christopher, R. Koppmann, O. Dubovik, D. P. Eleuterio, B. N. Holben, E. A. Reid, and J. Zhang (2005a), A review of biomass burning emissions part III: intensive optical properties of biomass burning particles, *Atmospheric Chemistry and Physics*, *5*, 827-849.
Reid, J. S., R. Koppmann, T. F. Eck, and D. P. Eleuterio (2005b), A review of biomass burning emissions part II: intensive physical properties of biomass burning particles, *Atmospheric Chemistry and Physics*, *5*, 799-825, doi:10.5194/acp-5-799-2005.
Reidmiller, D. R., D. A. Jaffe, E. V. Fischer, and B. Finley (2010), Nitrogen oxides in the boundary layer and free troposphere at the Mt. Bachelor Observatory, *Atmospheric Chemistry and Physics*, *10*(13), 6043-6062, doi:10.5194/acp-10-6043-2010.
Sakamoto, K., J. Allan, H. Coe, J. Taylor, T. Duck, and J. Pierce (2015), Aged boreal biomass-burning aerosol size distributions from BORTAS 2011, *Atmospheric Chemistry and Physics*, *15*(4), 1633-1646.
Sakamoto, K., J. Laing, R. Stevens, D. Jaffe, and J. Pierce (2016), The evolution of biomass-burning aerosol size distributions due to coagulation: dependence on fire and meteorological details and parameterization, *Atmos. Chem. Phys.*, *16*(12), 7709-7724, doi:10.5194/acp-16-7709-2016.
Seinfeld, J. H., and S. N. Pandis (2006), *Atmospheric Chemistry and Physics: From Air Pollution to Climate Change 2nd Edition*, John Wiley & Sons, Inc., Hoboken, New Jersey.
Spracklen, D. V., K. S. Carslaw, U. Poschl, A. Rap, and P. M. Forster (2011), Global cloud condensation nuclei influenced by carbonaceous combustion aerosol, *Atmospheric Chemistry and Physics*, *11*(17), 9067-9087, doi:10.5194/acp-11-9067-2011.
Stein, A. F., R. R. Draxler, G. D. Rolph, B. J. B. Stunder, M. D. Cohen, and F. Ngan (2015), NOAA'S HYSPLIT ATMOSPHERIC TRANSPORT AND DISPERSION MODELING SYSTEM, *Bulletin of the American Meteorological Society*, *96*(12), 2059-2077, doi:10.1175/bams-d-14-00110.1.
Stocks, B. J., et al. (1998), Climate change and forest fire potential in Russian and Canadian boreal forests, *Climatic Change*, *38*(1), 1-13, doi:10.1023/a:1005306001055.
Timonen, H., D. A. Jaffe, N. Wigder, J. Hee, H. Gao, L. Pitzman, and R. A. Cary (2014), Sources of carbonaceous aerosol in the free troposphere, *Atmospheric Environment*, *92*(0), 146-153, doi:http://dx.doi.org/10.1016/j.atmosenv.2014.04.014.

Timonen, H., N. Wigder, and D. Jaffe (2013), Influence of background particulate matter (PM) on urban air quality in the Pacific Northwest, *Journal of Environmental Management*, *129*, 333-340, doi:10.1016/j.jenvman.2013.07.023.

Vakkari, V., et al. (2014), Rapid changes in biomass burning aerosols by atmospheric oxidation, *Geophysical Research Letters*, *41*(7), 2644-2651, doi:10.1002/2014gl059396.

Virkkula, A. (2010), Correction of the Calibration of the 3-wavelength Particle Soot Absorption Photometer (3 PSAP), *Aerosol Science and Technology*, *44*(8), 706-712, doi:10.1080/02786826.2010.482110.

Virkkula, A., N. C. Ahlquist, D. S. Covert, W. P. Arnott, P. J. Sheridan, P. K. Quinn, and D. J. Coffman (2005), Modification, calibration and a field test of an instrument for measuring light absorption by particles, *Aerosol Science and Technology*, *39*, 68-83, doi:10.1080/027868290901963.

Weiss-Penzias, P., D. Jaffe, P. Swartzendruber, W. Hafner, D. Chand, and E. Prestbo (2007), Quantifying Asian and biomass burning sources of mercury using the Hg/CO ratio in pollution plumes observed at the Mount Bachelor Observatory, *Atmospheric Environment*, *41*(21), 4366-4379, doi:10.1016/j.atmosenv.2007.01.058.

Weiss-Penzias, P., D. A. Jaffe, P. Swartzendruber, J. B. Dennison, D. Chand, W. Hafner, and E. Prestbo (2006), Observations of Asian air pollution in the free troposphere at Mount Bachelor Observatory during the spring of 2004, *Journal of Geophysical Research-Atmospheres*, *111*(D10), D10304-D10304, doi:10.1029/2005JD006522.

Westerling, A. L., H. G. Hidalgo, D. R. Cayan, and T. W. Swetnam (2006), Warming and earlier Spring increase western U.S. forest wildfire activity, *Science*, *313*, 940-943.

Wiedinmyer, C., S. K. Akagi, R. J. Yokelson, L. K. Emmons, J. A. Al-Saadi, J. J. Orlando, and A. J. Soja (2011), The Fire INventory from NCAR (FINN): a high resolution global model to estimate the emissions from open burning, *Geoscience Model Development*, *4*, 625-641, doi:10.5194/gmd-4-625-2011.

Wigder, N. L., D. A. Jaffe, and F. A. Saketa (2013), Ozone and particulate matter enhancements from regional wildfires observed at Mount Bachelor during 2004-2011, *Atmospheric Environment*, *75*, 24-31, doi:10.1016/j.atmosenv.2013.04.026.

Winker, D. M., J. Pelon, J. Coakley Jr, S. Ackerman, R. Charlson, P. Colarco, P. Flamant, Q. Fu, R. Hoff, and C. Kittaka (2010), The CALIPSO mission: A global 3D view of aerosols and clouds, *Bulletin of the American Meteorological Society*, *91*(9), 1211.

Winker, D. M., M. A. Vaughan, A. Omar, Y. Hu, K. A. Powell, Z. Liu, W. H. Hunt, and S. A. Young (2009), Overview of the CALIPSO mission and CALIOP data processing algorithms, *Journal of Atmospheric and Oceanic Technology*, *26*(11), 2310-2323.

Yokelson, R. J., M. O. Andreae, and S. K. Akagi (2013a), Pitfalls with the use of enhancement ratios or normalized excess mixing ratios measured in plumes to characterize pollution sources and aging, *Atmospheric Measurement Techniques*, *6*, 2155-2158, doi:10.5194/amtd-6-4077-2013.

Yokelson, R. J., et al. (2013b), Coupling field and laboratory measurements to estimate the emission factors of identified and unidentified trace gases for prescribed fires, *Atmospheric Chemistry and Physics*, *13*(1), 89-116, doi:10.5194/acp-13-89-2013.

Yokelson, R. J., et al. (2009), Emissions from biomass burning in the Yucatan, *Atmospheric Chemistry and Physics*, *9*, 5785-5812, doi:10.5194/acp-9-5785-2009.

Table 1. Identified BB plumes at MBO during the summer of 2015. All enhancement ratios are obtained by taking the slope of a RMA linear regression between the two species. ND ("no data") indicates missing data. WC in the MAE column signifies a weak correlation ($R^2 < 0.60$).

Event number	Event date and time (UTC)	Event duration (hours)	Source fire location	ΔWV (g/kg)	$\Delta\sigma_{scat}/\Delta CO$ (Mm^{-1} ppbv^{-1})	$\Delta\sigma_{abs}/\Delta CO$ (Mm^{-1} ppbv^{-1})	MSE (m^2 g^{-1})	MAE (m^2 g^{-1})	AAE (467-660 nm)	ω (528 nm)	D_{pm} (nm)	σ_g
1	7/31/15 15:35-17:10	1.58	OR	0.16	1.13	0.036	ND	ND	3.15	0.97	164	1.72
2	8/9/15 2:55-8:55	6	CA, OR	1.62	0.89	WC	3.17	0.085	3.45	0.98	138	1.82
3	8/9/15 13:35-8/10/15 0:00	10.42	CA, OR	2.07	1.24	0.033	3.29	0.087	3.72	0.98	156	1.7
4	8/10/15 1:10-5:55	4.75	CA, OR	1.86	1.05	0.03	3.78	0.108	3.86	0.97	182	1.54
5	8/10/15 6:05-11:40	5.58	CA, OR	1.25	1.09	0.034	3.44	0.106	4.02	0.97	183	1.61
6	8/10/15 11:45-14:35	2.83	CA, OR	1.32	0.94	WC	3.27	WC	4.12	0.99	177	1.61
7	8/10/15 14:40- 8/11/15 6:15	15.58	CA, OR	1.83	1.17	0.032	3.64	0.098	3.52	0.98	186	1.62
8	8/11/15 14:20-18:45	4.42	CA, OR	1.11	1.07	0.029	2.5	0.066	2.74	0.98	160	1.78
9	8/14/15 10:00-15:35	5.58	OR	1.12	0.48	0.007	2.75	0.042	3.06	0.99	165	1.67
10	8/17/15 0:05-3:55	3.83	Siberia	-0.87	1.39	0.078	ND	ND	2.48	0.95	176	1.57
11	8/17/15 17:15- 8/18/15 7:00	13.75	Siberia	-0.22	1.06	0.060	ND	ND	2.5	0.95	179	1.69
12	8/18/15 16:05 - 8/19/15 16:40	24.58	Siberia	0.56	1.29	0.075	ND	ND	2.3	0.95	196	1.64
13	8/19/15 17:40 - 8/20/15 3:05	9.42	Siberia	0.6	1.12	0.052	ND	ND	2.25	0.96	175	1.76
14	8/22/15 15:30-18:05	2.58	Siberia	-3.1	1.97	0.078	4.76	0.188	3.59	0.96	229	1.73
15	8/23/15 3:55-7:00	3.08	Siberia	-2.45	1.09	0.059	2.84	0.156	2.51	0.96	162	1.89
16	8/23/15 9:50 - 8/25/15 6:50	45	CA, OR	1	1.13	0.029	4.06	0.107	3.15	0.98	205	1.58
17	8/25/15 12:45 - 8/26/15 19:00	30.25	CA, OR	1.67	0.88	0.027	3.75	0.111	3.12	0.98	181	1.6
18	8/26/15 7:15 - 8/28/15 11:15	40	CA, OR	1.35	0.89	0.031	3.7	0.128	3.48	0.97	191	1.53
19	8/28/15 17:40 - 8/29/15 6:15	12.58	CA, OR	1.54	0.69	ND	2.94	ND	ND	ND	164	1.58
Regional BB events (mean ± stdev)				1.38 ± 0.49	0.97 ± 0.21	0.03 ± 0.01	3.36 ± 1.03	0.09 ± 0.04	3.45 ± 1.04	5.71 ± 1.65	170 ± 15.7	1.67 ± 0.08
Siberian BB events (mean ± stdev)				-0.91 ± 1.56	1.32 ± 0.34	0.07 ± 0.01	3.8 ± 2.05	0.17 ± 0.09	2.61 ± 0.49	4.16 ± 0.6	181 ± 19.7	1.77 ± 0.1

ΔWV is water vapor enhancement, calculated for each event by subtracting the average WV for the summer sampling period from the WV value at the time when maximum CO was observed.

Aerosol scattering σ_{scat} (550 nm) and absorption σ_{abs} (528 nm) measurements were converted to STP.

MSE and MAE calculated as the $\Delta\sigma_{scat}/\Delta PM1$ and $\Delta\sigma_{abs}/\Delta PM1$enhancement ratios, respectively.

D_{pm} is the geometric mean diameter and σ_g is the geometric standard deviation of the SMPS aerosol size distribution.

WC indicates a weak correlation in the MAE column ($R^2 < 0.60$).

ND indicates missing data. PM data was not available for events 1 and 10-13; absorption data was not available for events 19 and 20.

Formatted: Width: 11", Height: 8.5"

Formatted Table

Formatted: Font: 9 pt

Formatted: Superscript

Formatted: Left

Formatted: Left

Formatted: Left

Formatted: Left

Formatted: Left

Formatted: Left

Formatted: Left

Formatted: Left

Formatted: Left

Formatted: Left

Event number	Event date and time (UTC)	Event duration (hours)	Source fire location	ΔWV (g/kg)	$\Delta\sigma_{scat}/\Delta CO$ (Mm^{-1}/ppbv)	$\Delta\sigma_{abs}/\Delta CO$ (Mm^{-1}/ppbv)	MSE (m^2/g)	MAE (m^2/g)	AAE (467-660 nm)	ω (528 nm)	D_{pm} (nm)	σ_g
1	7/31/15 15:35-17:10	1.58	OR	0.16	1.13	0.036	ND	ND	3.15	0.97	164	1.72
2	8/9/15 2:55-8:55	6.00	CA, OR	1.62	0.89	WC	3.17	0.085	3.45	0.98	138	1.82
3	8/9/15 13:35-8/10/15 0:00	10.42	CA, OR	2.07	1.24	0.033	3.29	0.087	3.72	0.98	156	1.70
4	8/10/15 1:10-5:55	4.75	CA, OR	1.86	1.05	0.030	3.78	0.108	3.86	0.97	182	1.54
5	8/10/15 6:05-11:40	5.58	CA, OR	1.25	1.09	0.034	3.44	0.106	4.02	0.97	183	1.61
6	8/10/15 11:45-14:35	2.83	CA, OR	1.32	0.94	WC	3.27	WC	4.12	0.99	177	1.61
7	8/10/15 14:40-8/11/15 6:15	15.58	CA, OR	1.83	1.17	0.032	3.64	0.098	3.52	0.98	186	1.62
8	8/11/15 14:20-18:45	4.42	CA, OR	1.11	1.07	0.029	2.50	0.066	2.74	0.98	160	1.78
9	8/14/15 10:00-15:35	5.58	OR	1.12	0.48	0.007	2.75	0.042	3.06	0.99	165	1.67
10	8/17/15 0:05-3:55	3.83	Siberian	0.87	1.39	0.078	ND	ND	2.48	0.95	176	1.57
11	8/17/15 17:15-8/18/15 7:00	13.75	Siberian	0.22	1.06	0.060	ND	ND	2.50	0.95	179	1.69
12	8/18/15 16:05-8/19/15 16:40	24.58	Siberian	0.56	1.29	0.075	ND	ND	2.30	0.95	196	1.64
13	8/19/15 17:40-8/20/15 3:05	9.42	Siberian	0.60	1.12	0.052	ND	ND	2.25	0.96	175	1.76
14	8/22/15 15:30-18:05	2.58	Siberian	3.10	1.97	0.078	4.76	0.188	3.59	0.96	229	1.73
15	8/23/15 3:55-7:00	3.08	Siberian	2.45	1.09	0.059	2.84	0.156	2.51	0.96	162	1.89
16	8/23/15 9:50-8/25/15 6:50	45.00	CA, OR	1.00	1.13	0.029	4.06	0.107	3.15	0.98	205	1.58
17	8/25/15 12:45-8/26/15 19:00	30.25	CA, OR	1.67	0.88	0.027	3.75	0.111	3.12	0.98	181	1.60
18	8/26/15 7:15-8/28/15 11:15	40.00	CA, OR	1.35	0.89	0.031	3.70	0.128	3.48	0.97	191	1.53
19	8/28/15 17:40-8/29/15 6:15	12.58	CA, OR	1.54	0.69	ND	2.94	ND	ND	ND	164	1.58

ΔWV is water vapor enhancement, calculated for each event by subtracting the average WV for the summer sampling period from the WV value at the time when maximum CO was observed.

Aerosol scattering σ_{scat} (550 nm) and absorption σ_{abs} (528 nm) measurements were converted to STP.

MSE and MAE calculated as the $\Delta\sigma_{scat}/\Delta PM1$ and $\Delta\sigma_{abs}/\Delta PM1$ enhancement ratios, respectively.

D_{pm} is the geometric mean diameter and σ_g is the geometric standard deviation of the SMPS aerosol size distribution.

WC indicates a weak correlation in the MAE column ($R^2 < 0.60$).

ND indicates missing data. PM data was not available for events 1 and 10-13; absorption data was not available for events 19 and 20.

Figures:

Formatted: Space After: 8 pt, Line spacing: Multiple 1.08 li

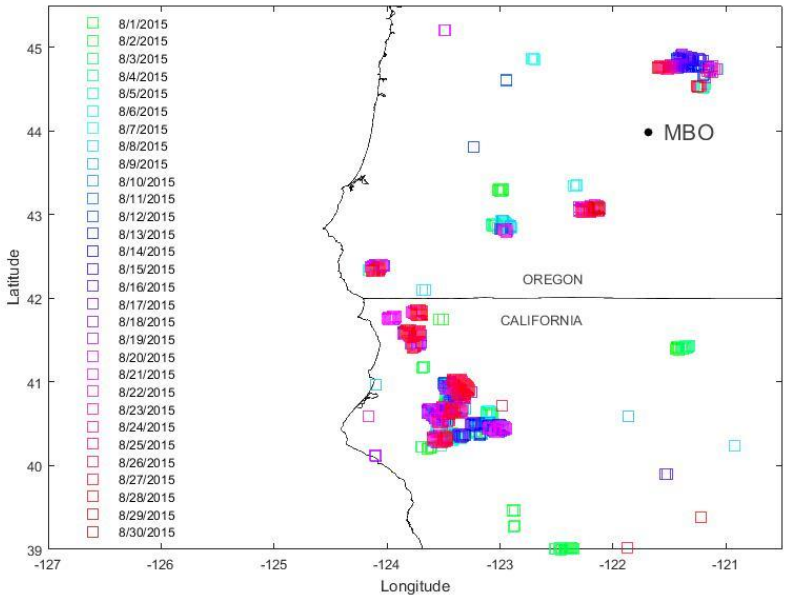

910 **Figure 1.** MBO and MODIS firespots colored by date for the month of August.

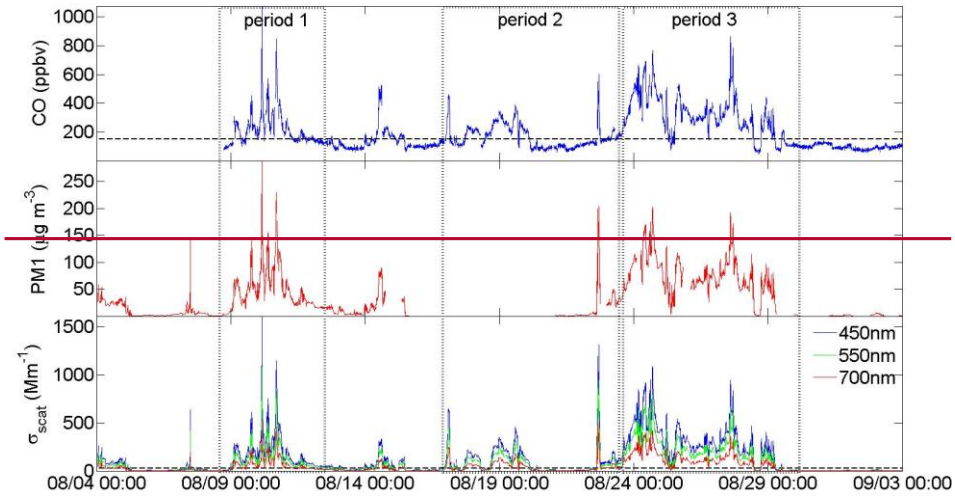
period 1
period 2
period 3
CO (ppbv)
PM1 (μg m-3)
σscat (Mm-1)
450nm
550nm
700nm
08/04 00:00
08/09 00:00
08/14 00:00
08/19 00:00
08/24 00:00
08/29 00:00
09/03 00:00

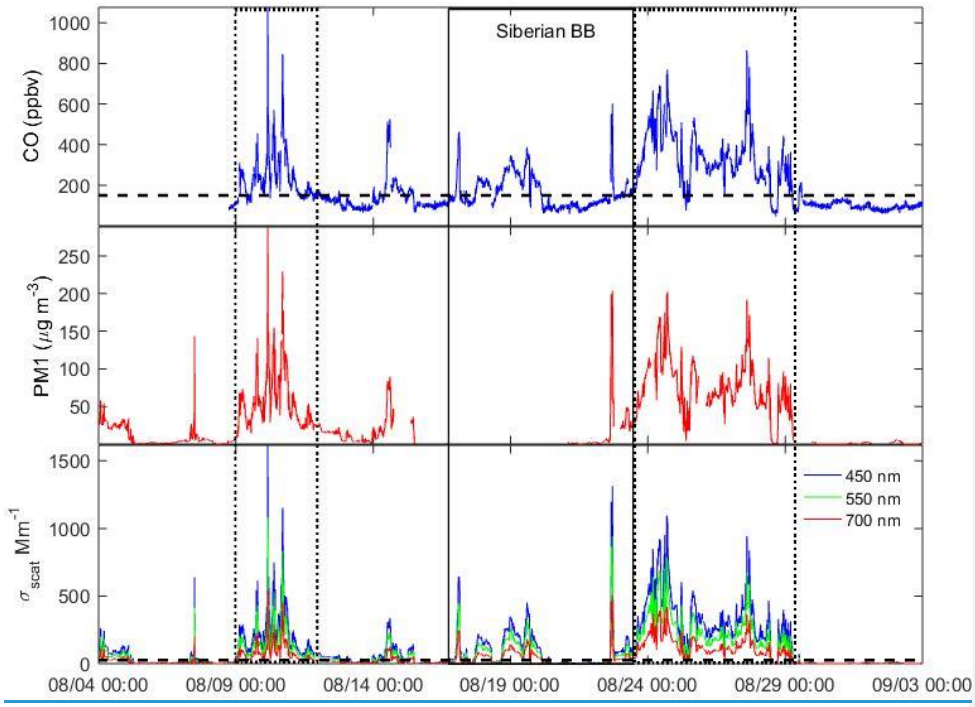
Siberian BB
CO (ppbv)
PM1 (μg m-3)
σscat Mm-1
450 nm
550 nm
700 nm
08/04 00:00
08/09 00:00
08/14 00:00
08/19 00:00
08/24 00:00
08/29 00:00
09/03 00:00

Figure 2. Time series of ~~(i)~~ CO, ~~(ii)~~ PM1, and aerosol scattering (σ_{scat}) ~~(iii)~~ at MBO during August. Threshold values (dashed black lines) used for BB event criteria are displayed for CO (150 ppbv) and scattering (20 Mm^{-1}). The dotted boxes represent multi-day periods of regional BB and encompasses events 2-8 and 16-19, respectively. The solid box represents the period influenced by Siberian BB and encompasses events 10-15.

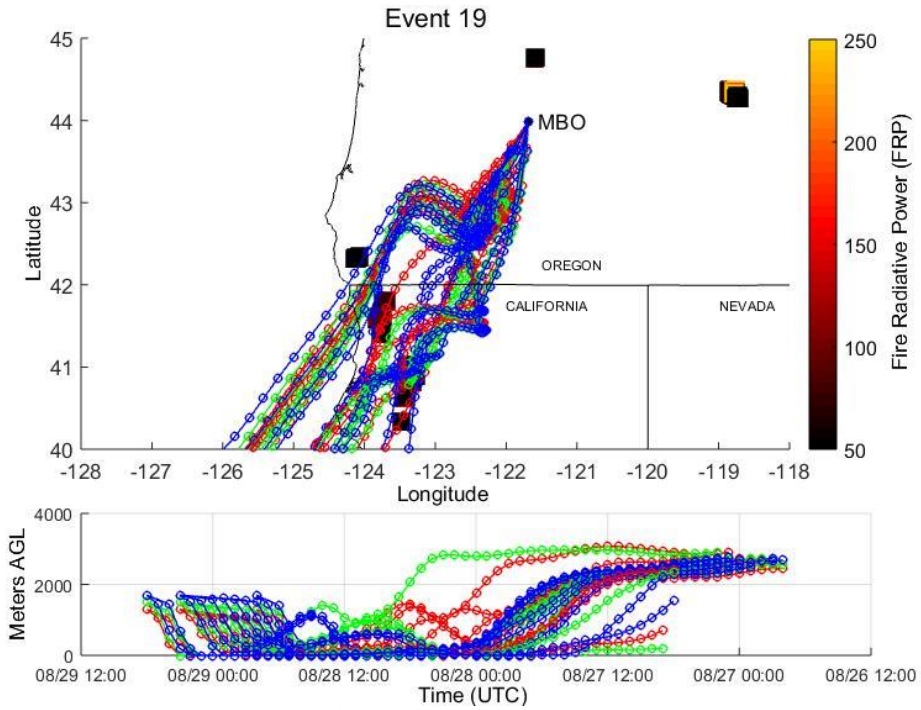

Figure 3. Hysplit Back-trajectories for Event 19. The blue back-trajectories have a starting height of 1700 m amgl (above model ground level)~~agl~~, the green a starting height of 1500 m amgl, and the red a starting height of 1300 m amgl. The squares are MODIS fire spots from 8/27/2015-8/29/2015 and are colored based on their fire radiative power (FRP). ~~**Three period are identified by dotted boxes. Periods 1 and 3 are regionally influenced and encompass events 2-8 and 16-19, respectively. Period 2 is influenced by Siberian BB and encompasses events 10-15.**~~

Formatted: Font: Bold

Formatted: Font: Not Bold

Formatted: Font: Bold

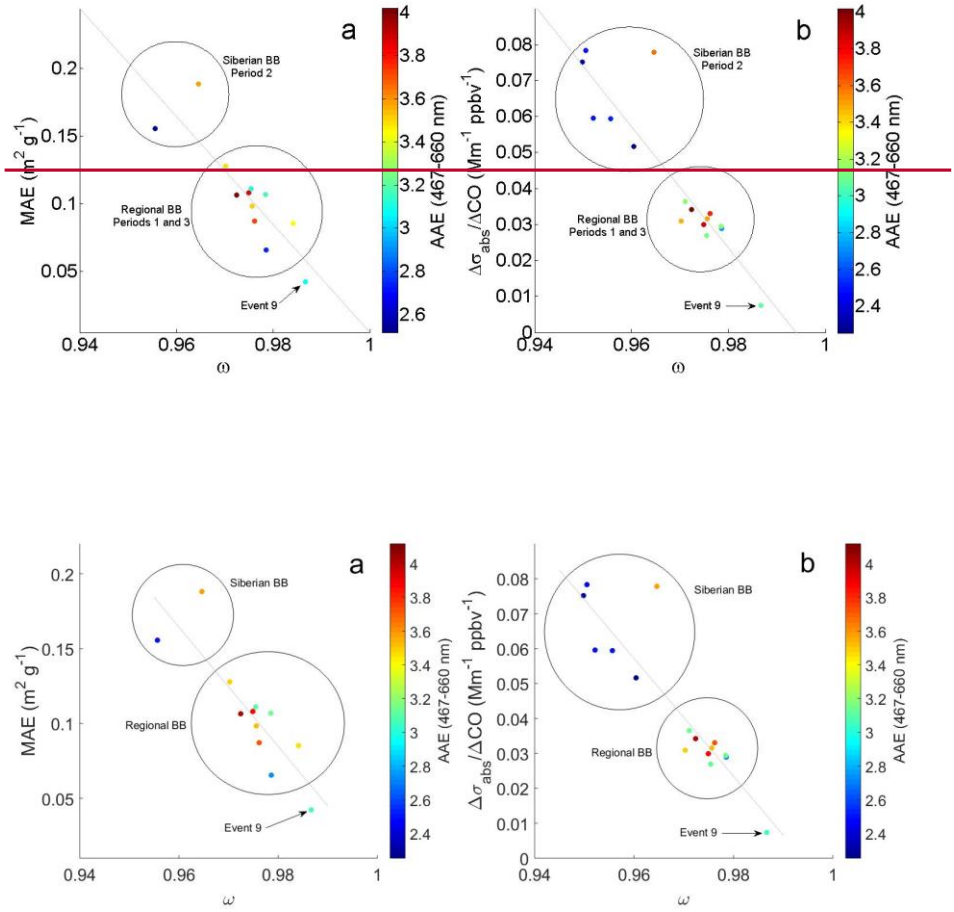

930

Figure 43. Scatter plots of (a) mass absorption efficiency (MAE) and (b) absorption enhancement ratio $\Delta\sigma_{abs}/\Delta CO$ versus single scattering albedo (ω). MAE values were not calculated for four of the six Siberian–influenced events due to missing PM1 data.

935

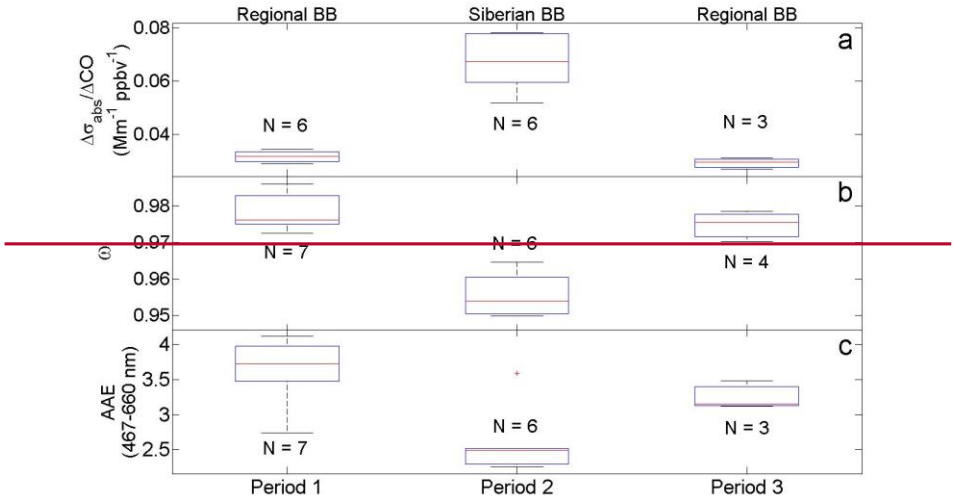
Regional BB
Siberian BB
Regional BB
a
b
c
N = 6
N = 6
N = 3
N = 7
N = 6
N = 4
N = 7
N = 6
N = 3
Period 1
Period 2
Period 3

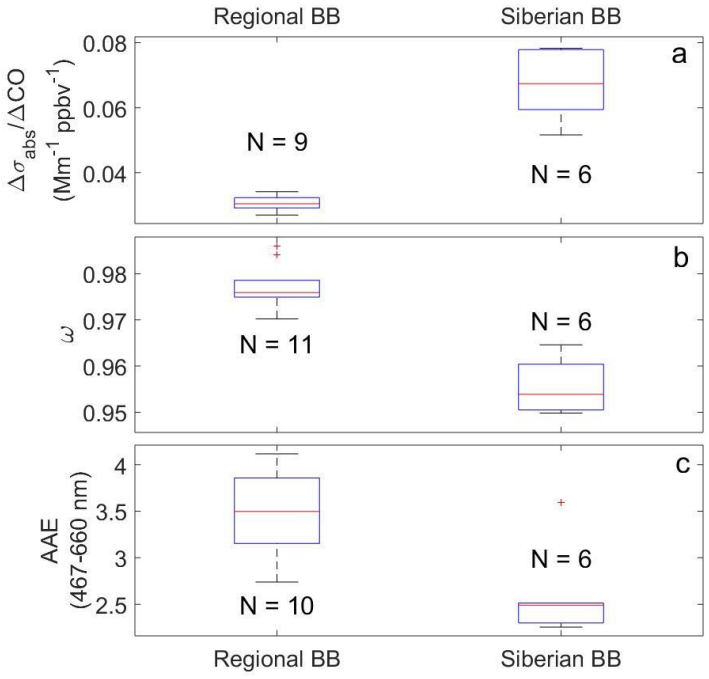
Regional BB
Siberian BB
a
b
c
N = 9
N = 6
N = 11
N = 6
N = 10
N = 6
Regional BB
Siberian BB

Figure 54. Boxplots of (a) $\Delta\sigma_{abs}/\Delta CO$, (b) single scattering albedo (ω) measured at 528 nm, and (c) ~~a~~Absorption Ångström exponent (AAE) for absorption measurements at 467 and 660 nm for regional BB events and Siberian influenced events. ~~the three periods shown in Figure 2. Periods 1 and 3 represent regional BB events, and period 2 consists of Siberian influenced events.~~ N indicates the number of events for each box. Lower and upper whiskers represent the minimum and maximum values, respectively. Lower and upper lines of the box represent the 25th and 75th percentiles, respectively. The red line ~~at~~in the middle of the box represents the median, and the red plus mark represents outliers.

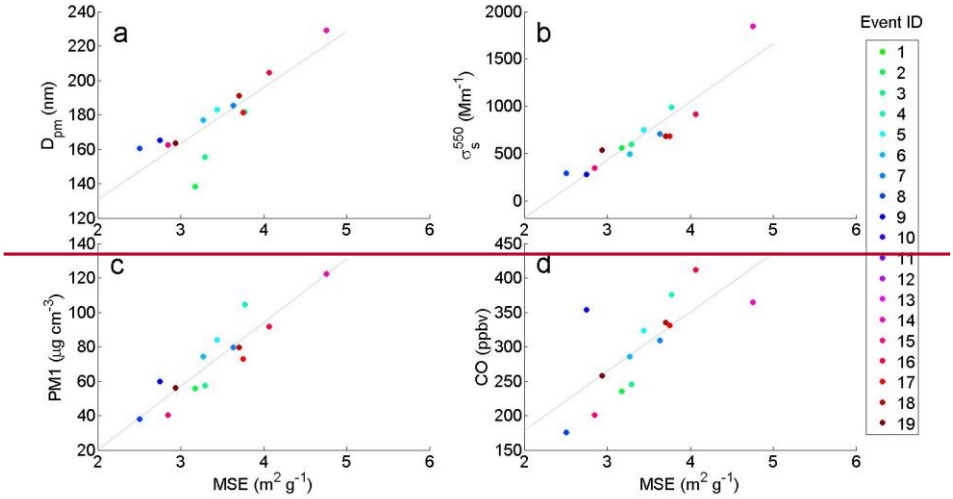

Figure 5. Scatter plots of (a) D_{pm} ($R^2 = 0.73$), (b) σ_{scat} ($R^2 = 0.90$), (c) PM1 ($R^2 = 0.85$), and (d) CO ($R^2 = 0.53$) versus mass scattering efficiency (MSE) for the BB events at MBO in the summer of 2015.

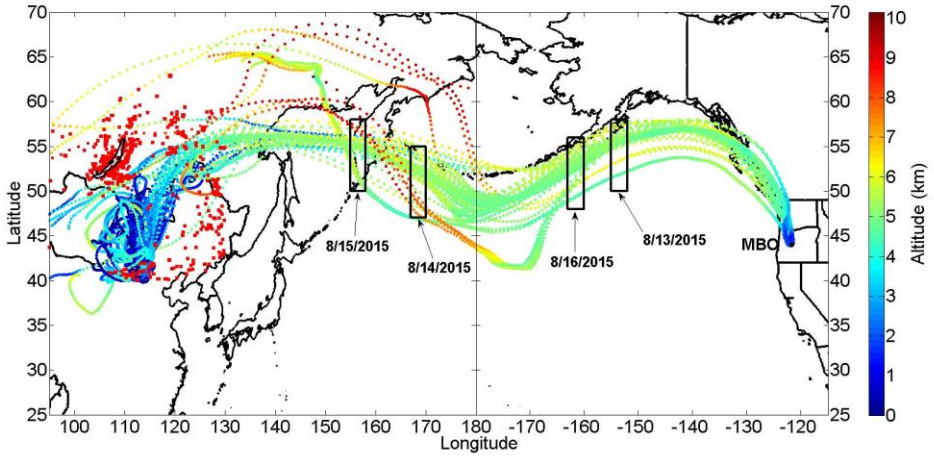

Figure 6. Most of the HYSPLIT back-trajectories for Siberian events (events 10-15) plotted as a function of altitude. Roughly 10% of the back-trajectories that did not follow the main transport track were not plotted. Forest fires from 8/7/2015 to 8/16/2015 identified by the Fire INventory from NCAR (FINN) fires are marked by red squares. These transects are not sequential and do not track one plume of Siberian smoke, but rather illustrate the extensive eastward transport of Siberian smoke over the course of the week. The four black boxes represent the locations of smoke plumes identified by CALIPSO cross sections detailed in Figures S~~2~~1-S~~5~~4.

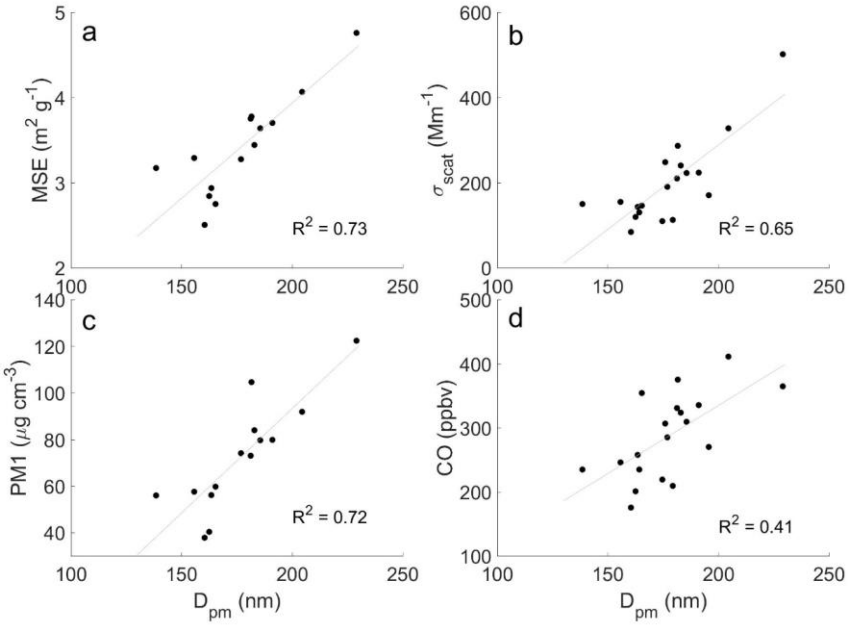

965 **Figure 7.** Scatter plots of (a) MSE, (b) σ_{scat}, (c) PM1, and (d) CO versus D_{pm} for the BB events at MBO in the summer of 2015.

Formatted: Space After: 8 pt, Line spacing: Multiple 1.08 li

970

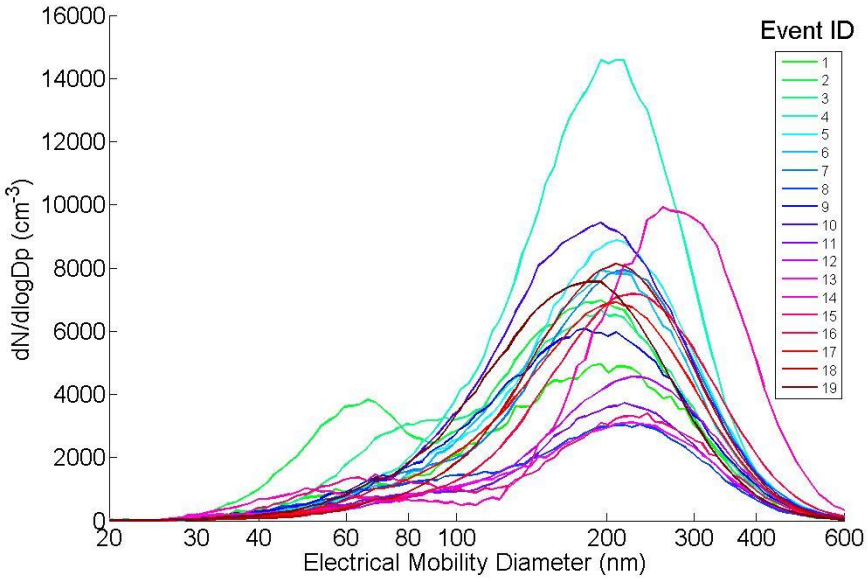

Figure 8~~6~~. Event integrated aerosol number size distributions (corrected to STP) in dN/dlogDp (# cm^{-1}).